

Generalizable Physics-Informed Learning for Stochastic Safety-Critical Systems

Zhuoyuan Wang, Albert Chern, Yorie Nakahira

Abstract—Accurate estimate of long-term risk is critical for safe decision-making, but sampling from rare risk events and long-term trajectories can be prohibitively costly. Risk gradient can be used in many first-order techniques for learning and control methods, but gradient estimate is difficult to obtain using Monte Carlo (MC) methods because the infinitesimal divisor may significantly amplify sampling noise. Motivated by this gap, we propose an efficient method to evaluate long-term risk probabilities and their gradients using short-term samples without sufficient risk events. We first derive that four types of long-term risk probability are solutions of certain partial differential equations (PDEs). Then, we propose a physics-informed learning technique that integrates data and physics information (aforementioned PDEs). The physics information helps propagate information beyond available data and obtain provable generalization beyond available data, which in turn enables long-term risk to be estimated using short-term samples of safe events. Finally, we demonstrate in simulation that the proposed technique has improved sample efficiency, generalizes well to unseen regions, and adapts to changing system parameters.

I. INTRODUCTION

Accurate estimation of long-term risk in stochastic systems is important as such information is key to designing safe control. Without accurate risk estimation, it is possible that one will misidentify or misclassify unsafe control policies as safe ones and compromise safety. Also, long outlook horizons are usually needed to plan far ahead enough to avoid unsafe regions of attraction in safety-critical control scenarios. However, to get accurate estimation of long-term risks is non-trivial and we summarize the challenges as below:

- *Lack of risky events.* The values of risk probability are often small in safety-critical systems, and thus huge amounts of sample trajectories are needed to capture the rare unsafe event.
- *Generalization in state space.* Since each point of interest requires one separate simulation, the sample complexity increases linearly with respect to the number of points needed for evaluation.
- *Generalization in time horizon.* Estimating long-term risk is computationally expensive, because the possible state trajectories scale exponentially with regard to the time horizon. Generalization to longer time horizon is challenging for sample-based methods since one needs to simulate the system for the entire horizon for evaluation.

Zhuoyuan Wang and Yorie Nakahira are with the Department of Electrical and Computer Engineering, Carnegie Mellon University, PA 15213 USA (e-mail: zhuoyuaw, ynakahir@andrew.cmu.edu).

Albert Chern is with the Department of Computer Science and Engineering, University of California San Diego, CA 92093 USA (e-mail: alchern@ucsd.edu).

- *Noisy estimation of probability gradients.* Estimating gradients of risk probabilities is difficult, as sampling noise is amplified by the infinitesimal divisor while taking derivatives over the estimated risk probabilities.

To resolve the abovementioned issues, we propose a physics-informed learning framework PIPE (Physics-Informed Probability Estimator) to estimate risk probabilities in an efficient and generalizable manner. Fig. 1 shows the overview diagram of the proposed PIPE framework. The framework consists of two key parts, namely the physics model part and the data-enabled learning part. For the former part, we derive that the evolution of risk probabilities given stochastic system dynamics and nominal controllers is governed by deterministic partial differential equations (PDEs). For the latter part, we integrate the physics model knowledge from the PDEs with sampled data to train a physics-informed neural network. The framework takes both data and physics models into consideration, and by combining the two, we achieve better sample efficiency and the ability to generalize to unseen regions in the state space and unknown parameters in the system dynamics. The resulting framework takes only inaccurate sample data in a sparse sub-region of the state space for training, and is able to accurately predict the risk probability and its gradient with reduced sample complexity over the whole state space for systems with different parameters.

The rest of the paper is organized as follows. In section II we list related work. In section III we give preliminaries. In section IV we state the problem formulation. In section V we derive the mathematical characterization of risk probability with partial differential equations. In section VI we present the proposed physics-informed learning framework for probability estimation. In section VII we show experiment results. Finally we conclude the paper in section VIII.

II. RELATED WORK

A. Risk Probability Estimation

Risk probabilities are estimated through rare event simulation or analytical approximation in the previous literature. For rare event simulation, risk in the system is estimated through the Monte Carlo (MC) method and its variants. Standard MC forward runs the system dynamics multiple times to empirically estimate the risk probability by calculating the unsafe trajectory numbers over the total trajectory number [1]. To improve sample complexity, importance sampling [2]–[4] and subset simulation [5] are used on top of standard MC. However, computational efficiency remains an issue and

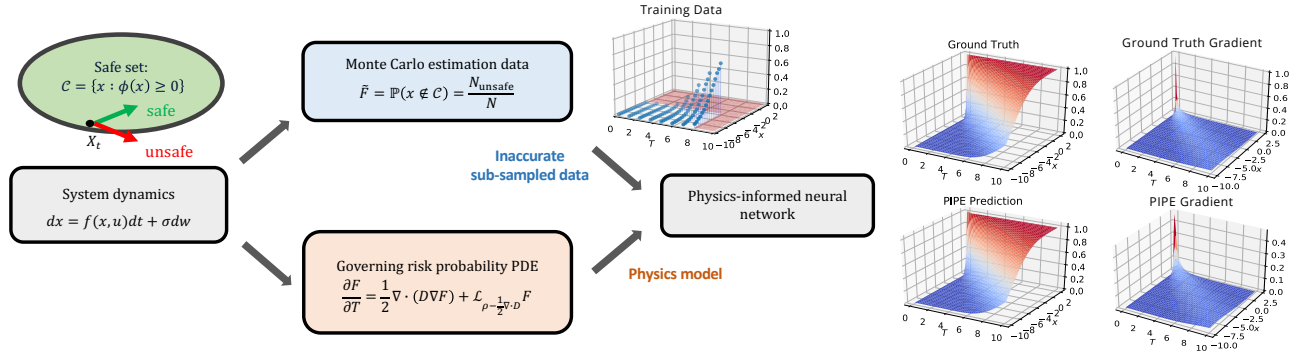


Fig. 1: The overview diagram of the proposed PIPE framework. The system takes form (1) with safe set defined as (3). For training data, one can acquire the empirical risk probabilities by simulating the system dynamics and calculating the ratio of unsafe trajectories over all trajectories, without the need to cover the entire time-state space (shaded red region has no training data). For the physics model, we derive that the mapping between state-time pair and the risk probability satisfies a governing convection diffusion equation (Theorem 1-4). The PIPE framework uses physics-informed neural networks to learn the risk probability by fitting the empirical training data and using the physics model as constraints. PIPE gives more accurate and sample efficient risk probability and gradient predictions than Monte Carlo or its variants, and can generalize to unseen regions in the state space and unknown parameters in the system dynamics thanks to its integration of data and physics models.

generalization to the entire state space is hard to achieve, as the estimation can only be conducted at a single point once [6].

For analytical approximation, previous studies provide insightful bounds for safe possibilities [7]–[11]. Their analysis commonly uses probability bounds, martingale inequalities, and characterization of tail distributions, and conversion into deterministic worst-case settings, which may yield loose approximations for certain cases. Such loose approximations may lead to unnecessarily conservative control actions that compromise performance.

Opposed to previous work, our proposed method derives the exact distributions for the risk probabilities in a time interval through the solutions of PDEs, which can be efficiently solved by the physics-informed neural networks.

B. Physics-informed Neural Networks

Physics-informed neural networks (PINNs) are neural networks that are trained to solve supervised learning tasks while respecting any given laws of physics described by general non-linear partial differential equations [12]–[14]. PINNs take both data and the physics model of the system into account, and are able to solve the forward problem of getting PDE solutions, and the inverse problem of discovering underlying governing PDEs from data. PINNs have been widely used in power systems [15], fluid mechanics [16] and medical care [17]. Different variants of PINN have been proposed to meet different design criteria, for example Bayesian physics-informed neural networks are used for forward and inverse PDE problems with noisy data [18], physics-informed neural networks with hard constraints are proposed to solve topology optimizations [19], and parallel physics-informed neural networks via domain decomposition are proposed to solve multi-scale and multi-physics problems [20]. Theoretical guarantees in terms of approximation error [21]–[24], generalization error [25]–[28], and convergence rate [29]–[31] are also studied in previous

literature. For stochastic control, previous works use PINNs to solve the initial value problem of deep backward stochastic differential equations to derive an end-to-end myopic safe controller [32]. However, to the best of our knowledge there is no work that considers PINNs for risk probability estimation, especially on the full state-time space scale. In this work, we take the first step towards leveraging PINNs on the problem of risk probability estimation.

C. Neural Network Gradient Estimation

Estimating gradients of neural network output by itself is an important research topic as the gradients are essential for characterizing complex natural signals. There are two lines of work in estimating the gradients of neural network, which are directly estimating functional gradients, and estimating functions while obtaining gradients through certain mechanism such as automatic differentiation. For the first line of work, monotone gradient networks are studied to learn the gradients of convex functions [33]. For the second line of work, backward propagation is used as a standard method to calculate gradients of neural network output with regard to its input [34], [35], and implicit neural representations with periodic activation functions have shown its efficacy in characterizing higher-order gradients of neural network outputs [36], [37]. Our proposed framework aligns with the second line of work, where accurate probability gradients are obtained through automatic differentiation once the neural network is trained.

D. Potential Applications

Accurate estimation of long-term risk and safety probabilities can be crucial to a lot of safety-critical control and learning applications. For example, for safe control, chance-constrained predictive control takes probabilistic safety requirements as the constraints in an optimization-based controller, and solves

a minimal distance control to a nominal controller to find its safe counterpart [38]–[40]. For safe learning, probabilistic safety certificate can ensure long-term safety of neural network-based controller through forward invariance on the probability space [41]. For safe reinforcement learning, the probabilistic safety certificate can safe guard reinforcement learning agents during and after training [42]–[45] (*e.g.*, policy gradient and Q-learning agents [44]), and similar frameworks can be potentially used in meta learning settings as well [46]. While these methods provide safety guarantees, most of them will require accurate estimation of risk probabilities or their gradients to yield desirable performance, and to get accurate estimates itself challenging. We tackle this problem by combining physics models and data to provide accurate estimates of risk probability and its gradient.

III. PRELIMINARIES

Let \mathbb{R} , \mathbb{R}_+ , \mathbb{R}^n , and $\mathbb{R}^{m \times n}$ be the set of real numbers, the set of non-negative real numbers, the set of n -dimensional real vectors, and the set of $m \times n$ real matrices. Let $x[k]$ be the k -th element of vector x . Let $x^+ = \max(x, 0)$ and $x \wedge y = \min\{x, y\}$ for $x, y \in \mathbb{R}$. Let $f : \mathcal{X} \rightarrow \mathcal{Y}$ represent that f is a mapping from space \mathcal{X} to space \mathcal{Y} . Let $\mathbb{1}_{\mathcal{E}}$ be an indicator function, which takes 1 when condition \mathcal{E} holds and 0 otherwise. Let $\mathbb{P}_x(\mathcal{E}) = \mathbb{P}(\mathcal{E}(X)|X_0 = x)$ denote the probability of event $\mathcal{E}(X)$ involving a stochastic process $X = \{X_t\}_{t \in \mathbb{R}_+}$ conditioned on $X_0 = x$. Let $\mathbb{E}_x[F(X)] = \mathbb{E}[F(X)|X_0 = x]$ denote the expectation of $F(X)$ (a functional of X) conditioned on $X_0 = x$. We use upper-case letters (*e.g.*, X) to denote random variables and lower-case letters (*e.g.*, x) to denote their specific realizations.

IV. PROBLEM STATEMENT

We present the settings and the scope of this paper in section IV-A and section IV-B, respectively.

A. System Description and design specifications

We consider a control system with stochastic noise of k -dimensional Brownian motion W_t starting from $W_0 = 0$. The system state, $X_t \in \mathbb{R}^n, t \in \mathbb{R}_+$, evolves according to the following stochastic differential equation (SDE)

$$dX_t = (f(X_t) + g(X_t)U_t)dt + \sigma(X_t)dW_t, \quad (1)$$

where $U_t \in \mathbb{R}^m$ is the control input. Throughout this paper, we assume sufficient regularity in the coefficients of the SDE (1). That is, $f, g, (U_t)_{t \in \mathbb{R}_+}$ are chosen in a way such that there exist a unique strong solution to (1).¹ The state of the system X_t can contain both the state of the plant, which can be controlled, and the state of environmental variables (*e.g.*, moving obstacles), which cannot be controlled.² The size of $\sigma(X_t)$ is determined from the uncertainties in the disturbance,

¹See [47, Chapter 1], [48, Chapter II.7] and references therein for required conditions.

²Let X_p be the state of the plant to be controlled and X_o be the environmental variables which cannot be controlled. The dynamics of X_p and X_o can be jointly captured by a system with the augmented state space $X^\top = [X_p^\top, X_o^\top]$.

unmodeled dynamics [11], and the prediction errors of the environmental variables [49], [50]. Examples of these cases include when the unmodeled dynamics are captured using statistical models such as Gaussian Processes [11]³ and when the motion of the environment variables are estimated using physics-based models such as Kalman filters [49], [50].

The control signal is generated by a memoryless state feedback controller of the form

$$U_t = K(X_t). \quad (2)$$

Examples of controllers of this form include classic controllers (*e.g.*, PID), optimization-based controllers (*e.g.*, some robust controllers and nonlinear controllers), safe control methods [7]–[11], [51], and some hybrid of those.

One of the major design considerations for K is system safety. This in turn requires a rigorous analysis on the following two aspects related to safety: forward invariance and recovery. The forward invariance refers to the property that the system state always stays in the safe region, while recovery refers to the property that the system state recovers to the safe region even if it originates from the unsafe region.

Definition 1 (Safe Set). The safe region is defined using a set \mathcal{C} that is characterized by a super level set of some function $\phi(x)$, *i.e.*,

$$\mathcal{C} = \{x \in \mathbb{R}^n : \phi(x) \geq 0\}, \quad (3)$$

We call \mathcal{C} the *safe set*, and $\phi(x)$ the barrier function. Additionally, we denote the boundary of the safe set and unsafe set by

$$\partial\mathcal{C} = \{x \in \mathbb{R}^n : \phi(x) = 0\}, \quad (4)$$

$$\mathcal{C}^c = \{x \in \mathbb{R}^n : \phi(x) < 0\}. \quad (5)$$

We assume that $\phi(x) : \mathbb{R}^n \rightarrow \mathbb{R}$ is a second-order differentiable function whose gradient does not vanish at $\partial\mathcal{C}$.

We assume that the dynamics and uncertainty in the control system and the environment (*e.g.*, uncertainties in the environment and moving obstacles) are all captured in (1)² so that the safe set can be defined using a static function $\phi(x)$ instead of a time-varying one.

1) *Forward invariance*: When the initial state starts from a safe region, *i.e.*, $X_0 = x \in \mathcal{C}$, we study the quantities associated with forward invariance: the safety margin from $\partial\mathcal{C}$ and the first exit time from \mathcal{C} .

Properties associated invariance to a set have been studied from the perspective of forward invariance. A forward invariant set with respect to a system is often defined to satisfy $X_0 \notin \mathcal{M} \Rightarrow X_t \in \mathcal{M}, \forall t \in \mathbb{R}_+$ in a deterministic framework [52, Section 4.2]. However, in a stochastic system, it may not be always possible to ensure $X_t \in \mathcal{M}$ at all time because the probability of exiting \mathcal{M} can accumulate over time.⁴ Therefore, we use a modified definition, formally defined below, where $X_t \in \mathcal{M}$ is only required to hold in a finite time interval T .

³In such settings, the value of $\sigma(X_t)$ can be determined from the output of the Gaussian Process.

⁴From Theorem 1, it can be shown that $\mathbb{P}(\Theta_x(T) \geq 0) \rightarrow 0$ as $T \rightarrow \infty$ in many cases.

Definition 2 (Forward Invariance). The state of system (1) is said to remain forward invariant with respect to a set \mathcal{M} during a time interval $[0, T]$ if, given $X_0 = x \in \mathcal{M}$,

$$X_t \in \mathcal{M}, \quad \forall t \in (0, T]. \quad (6)$$

We study the probability of forward invariance to the safe set through characterizing the distributions of the following two random variables:

$$\Phi_x(T) := \inf\{\phi(X_t) \in \mathbb{R} : t \in [0, T], X_0 = x\}, \quad (7)$$

$$\Gamma_x(\ell) := \inf\{t \in \mathbb{R}_+ : \phi(X_t) \leq \ell, X_0 = x\}, \quad (8)$$

where $x \in \mathcal{C}$. The value of $\Phi_x(T)$ informs the worst-case safety margin from the boundary $\partial\mathcal{C}$ during $[0, T]$, while the value of $\Gamma_x(0)$ is the first exit time from the safe set.

The probability of staying within the safe set \mathcal{C} during a time interval $[0, T]$ given $X_0 = x \in \mathcal{C}$ can be computed using the distributions of (7) or (8) as

$$\begin{aligned} \mathbb{P}_x(X_t \in \mathcal{C}, \forall t \in [0, T]) &= \mathbb{P}(\Phi_x(T) \geq 0) \\ &= 1 - \mathbb{P}(\Gamma_x(0) \leq T). \end{aligned} \quad (9)$$

2) *Recovery*: When the initial state is outside of the safe region, i.e., $X_0 = x \notin \mathcal{C}$, we study the quantities associated with recovery: the distance from \mathcal{C} and the recovery time.

Properties associated with entrance to a set have been studied from the perspective of stochastic stability in different contexts. Stochastic stability is defined by, given \mathcal{M} , the existence of a set \mathcal{M}_0 such that $x_0 \in \mathcal{M}_0 \Rightarrow x_t \in \mathcal{M}, \forall t \geq 0$ with probability one [53, Chapter 2]. Here, stochastic stability requires invariance with probability one, and the invariance only need to hold for some set of (not all) initial conditions. However, stochastic stability is not applicable in our setting for two reasons: the state rarely stays in a set indefinitely after reaching it; and the initial state is often predetermined and cannot be chosen.⁴ Instead, we consider a weaker notion than stability, formally defined below, which requires re-entry for any initial condition but does not require invariance upon re-entry.

Definition 3 (Forward Convergent Set). A set \mathcal{M} is said to be a forward convergent set with respect to system (1) if

$$X_0 \notin \mathcal{M} \Rightarrow \exists \tau \in (0, \infty) \text{ s.t. } X_\tau \in \mathcal{M}. \quad (10)$$

That is, for any initial state that does not belong to set \mathcal{M} , the state re-enters the set in finite time. Equivalently, even if the state does not belong to set \mathcal{M} at some time, it will enter \mathcal{M} in finite time.⁵ Note that a forward convergent set does not require the state to stay in the set indefinitely after re-entry.

We study forward convergence to the safe set through characterizing the distribution of the following two random variables:

$$\Theta_x(T) := \sup\{\phi(X_t) \in \mathbb{R} : t \in [0, T], X_0 = x\}, \quad (11)$$

$$\Psi_x(\ell) := \inf\{t \in \mathbb{R}_+ : \phi(X_t) \geq \ell, X_0 = x\}, \quad (12)$$

⁵This equivalence holds with respect to (1) when the system parameters f, g, σ , and control policy K are time-invariant mappings.

where $x \notin \mathcal{C}$. The value of $\Theta_x(T)$ informs the distance⁶ to the safe set, while the recovery time $\Psi_x(0)$ is the duration required for the state to re-enter the safe region for the first time.

The probability of having re-entered the safe set \mathcal{C} by time T given $X_0 = x \notin \mathcal{C}$ can be computed using the distributions of (11) or (12) as

$$\begin{aligned} \mathbb{P}_x(\exists t \in [0, T] \text{ s.t. } X_t \in \mathcal{C}) &= \mathbb{P}(\Theta_x(T) \geq 0) \\ &= 1 - \mathbb{P}(\Psi_x(0) \leq T). \end{aligned} \quad (13)$$

More generally, the distributions of $\Phi_x(T)$, $\Theta_x(T)$, $\Gamma_x(\ell)$, and $\Psi_x(\ell)$ contain much richer information than the probability of forward invariance or recovery. Thus, knowing their exact distributions allows uncertainty and risk to be rigorously quantified in autonomous control systems.

B. Objective and scope of this paper

In this paper, we build upon analysis tools from stochastic processes to answer the following question:

- When certain control methods are used for the stochastic system (1), what are the *exact distributions* of (7), (8), (11), and (12)?
- With the characterization of the exact distribution of (7), (8), (11), and (12), how do we efficiently calculate them?

We will answer the first question in section V and the second question in section VI. The distribution of (7) and (8) will allow us to study the property of invariance from a variety of perspectives, such as the average failure time, the tail distributions of safety or loss of safety, and the mean and tail of the safety margin. The distribution of (11) and (12) will allow us to study the property of recovery from a variety of perspectives, such as the average recovery time, tail distribution of recovery, and the mean and tail distribution of recovery vs. crashes. The efficient calculation of (7), (8), (11), and (12) will allow us to design online stochastic safe control methods with probabilistic guarantees [41].

V. CHARACTERIZATION OF PROBABILITIES

In this section, we study the properties associated with safety (forward invariance) and recovery (forward convergence). The former is quantified using the distribution of the safety margin (7) and first exit time (8) in section V-A. The latter is quantified using the distribution of the distance to the safe set (11) and the recovery time (12) in section V-B.

The random variables of our interests, (7), (8), (11) and (12), are functions of $\phi(X_t)$. Since the stochastic dynamics of $d\phi(X_t)$ are driven by X_t , we consider the augmented state space

$$Z_t := \begin{bmatrix} \phi(X_t) \\ X_t \end{bmatrix} \in \mathbb{R}^{n+1}. \quad (14)$$

From Itô's lemma, dynamics of $\phi(X_t)$ satisfies

$$d\phi(X_t) = A\phi(X_t)dt + \mathcal{L}_\sigma\phi(X_t)dW_t. \quad (15)$$

⁶Here, we refer to distance with a slightly light abuse of notation as the value of $\Theta_x(\ell)$, $\Phi_x(\ell)$ measure the value of function ϕ , instead of the distance between a state x to the safe set \mathcal{C} . Note that the following condition holds: $\phi(x) \geq 0 \Leftrightarrow \text{Dist}(x, \mathcal{C}) := \inf_{y \in \mathcal{C}} \|x - y\| = 0$.

Combining (1) and (15), the dynamics of Z_t are given by the SDE

$$dZ_t = \rho(Z_t) dt + \zeta(Z_t) dW_t, \quad (16)$$

where the drift and diffusion parameters are

$$\rho(z) = \begin{bmatrix} D_\phi(x, K(x)) \\ (f(x) + g(x)K(x)) \end{bmatrix}, \quad \zeta(z) = \begin{bmatrix} \mathcal{L}_\sigma \phi(x) \\ \sigma(x) \end{bmatrix}. \quad (17)$$

Here, the mapping K is any nominal control policy of interest. Since risk probabilities are complementary to safety probabilities, we will consider four safety-related probabilities of interest in section V-A and section V-B. We will call them risk probabilities for simplicity.

Before presenting our main theorems on characterization of risk probabilities, we point out that our analysis can be applied to any closed-loop control systems whose augmented state space Z in (14) is the solution to the SDE (16) with appropriate regularity conditions.¹ The proof of all theorems can be found in the appendix of the paper.

A. Probability of Forward Invariance

When the state initiates inside the safe set, the distribution of the safety margin, $\Phi_x(T)$ in (7), is given below.

Theorem 1. Consider system (1) with the initial state $X_0 = x$. Let $z = [\phi(x), x^\top]^\top \in \mathbb{R}^{n+1}$. Then, the complementary cumulative distribution function (CCDF) of $\Phi_x(T)$,⁷

$$F(z, T; \ell) = \mathbb{P}(\Phi_x(T) \geq \ell), \quad \ell \in \mathbb{R}, \quad (18.A)$$

is the solution to the initial-boundary-value problem of the convection-diffusion equation on the super-level set $\{z \in \mathbb{R}^n : z[1] \geq \ell\}$

$$\begin{cases} \frac{\partial F}{\partial T} = \frac{1}{2} \nabla \cdot (D \nabla F) + \mathcal{L}_{\rho - \frac{1}{2} \nabla \cdot D} F, & z[1] \geq \ell, T > 0, \\ F(z, T; \ell) = 0, & z[1] < \ell, T > 0, \\ F(z, 0; \ell) = \mathbb{1}_{\{z[1] \geq \ell\}}(z), & z \in \mathbb{R}^{n+1}, \end{cases} \quad (18.B)$$

where $D := \zeta \zeta^\top$.⁸

Theorem 1 converts the problem of characterizing the distribution function into a deterministic convection-diffusion problem. When we set $\ell = 0$, it gives the exact probability that \mathcal{C} is a forward invariant set with respect to (1) during the time interval $[0, T]$. For arbitrary $\ell > 0$, it can be used to compute the probability of maintaining a safety margin of ℓ during $[0, T]$.

Moreover, the distribution of the first exit time from the safe set, $\Gamma_x(0)$ in (8), and the first exit time from an arbitrary super level set $\{x \in \mathbb{R}^n : \phi(x) \geq \ell\}$, is given below.

⁷We use CDFs and CCDFs with a slight abuse of notation. The presence or absence of equality in the inequality conditions are chosen so that the obtained probability can be used to compute (9) and (13). Also, note that if a random variable Y has a PDF, then $\mathbb{P}(Y \leq \ell) = \mathbb{P}(Y < \ell)$, so the presence or absence of equality in the probability density function does not affect the computed probabilities.

⁸Here, the spatial derivatives ∇ and \mathcal{L} apply to the variable $z \in \mathbb{R}^{n+1}$.

Theorem 2. Consider system (1) with the initial state $X_0 = x$. Let $z = [\phi(x), x^\top]^\top \in \mathbb{R}^{n+1}$. Then, the cumulative distribution function (CDF) of the first exit time $\Gamma_x(\ell)$,⁷

$$G(z, T; \ell) = \mathbb{P}(\Gamma_x(\ell) \leq T), \quad (19.A)$$

is the solution to

$$\begin{cases} \frac{\partial G}{\partial T} = \frac{1}{2} \nabla \cdot (D \nabla G) + \mathcal{L}_{\rho - \frac{1}{2} \nabla \cdot D} G, & z[1] \geq \ell, T > 0, \\ G(z, T; \ell) = 1, & z[1] < \ell, T > 0. \\ G(z, 0; \ell) = \mathbb{1}_{\{z[1] < \ell\}}(z), & z \in \mathbb{R}^{n+1}, \end{cases} \quad (19.B)$$

where $D = \zeta \zeta^\top$.⁸

Similarly, Theorem 2 gives the distribution of the first exit time from an arbitrary super level set of barrier function as the solution to a deterministic convection-diffusion equation. When we set $\ell = 0$, it can also be used to compute the exact probability of staying within the safe set during any time interval.

B. Probability of Forward Convergence

When the state initiates outside the safe set, the distribution of the distance from the safe set, $\Theta_x(T)$ in (11), is given below.

Theorem 3. Consider system (1) with the initial state $X_0 = x$. Let $z = [\phi(x), x^\top]^\top \in \mathbb{R}^{n+1}$. Then, the CDF of $\Theta_x(T)$,⁷

$$Q(z, T; \ell) = \mathbb{P}(\Theta_x(T) < \ell), \quad \ell \in \mathbb{R}, \quad (20.A)$$

is the solution to

$$\begin{cases} \frac{\partial Q}{\partial T} = \frac{1}{2} \nabla \cdot (D \nabla Q) + \mathcal{L}_{\rho - \frac{1}{2} \nabla \cdot D} Q, & z[1] < \ell, T > 0, \\ Q(z, T; \ell) = 0, & z[1] \geq \ell, T > 0, \\ Q(z, 0; \ell) = \mathbb{1}_{\{z[1] < \ell\}}(z), & z \in \mathbb{R}^{n+1}, \end{cases} \quad (20.B)$$

where $D = \zeta \zeta^\top$.⁸

Theorem 3 gives the distribution of safety distance $\Theta_x(T)$ as a deterministic convection-diffusion problem. When we set $\ell = 0$, it provides the exact probability that a stochastic process (1) initiating outside the safe set enters the safe set during the time interval $[0, T]$. When we set $\ell < 0$, it can be used to compute the probability of coming close to $|\ell|$ -distance from the safe set along the time interval $[0, T]$.

Finally, the distribution of the recovery time from the unsafe set, $\Psi_x(0)$ in (12), and the entry time to an arbitrary super level set of the barrier function, $\Psi_x(\ell)$, is given below.

Theorem 4. Consider system (1) with the initial state $X_0 = x$. Let $z = [\phi(x), x^\top]^\top \in \mathbb{R}^{n+1}$. Then, the CDF of the recovery time $\Psi_x(\ell)$,⁷

$$N(z, T; \ell) = \mathbb{P}(\Psi_x(\ell) \leq T), \quad (21.A)$$

is the solution to

$$\begin{cases} \frac{\partial N}{\partial T} = \frac{1}{2} \nabla \cdot (D \nabla N) + \mathcal{L}_{\rho - \frac{1}{2} \nabla \cdot D} N, & z[1] < \ell, T > 0, \\ N(z, T; \ell) = 1, & z[1] \geq \ell, T > 0, \\ N(z, 0; \ell) = \mathbb{1}_{\{z[1] \geq \ell\}}(z), & z \in \mathbb{R}^{n+1}, \end{cases} \quad (21.B)$$

where $D = \zeta\zeta^\top$.⁸

Theorem 4 gives the distribution of the re-entry time as a solution to a deterministic convection-diffusion equation. When we set $\ell = 0$, it can be used to compute the exact probability of entering the safe region during any time intervals. When we set $\ell < 0$, it can be used to study the first time to reach $|\ell|$ -close to the safe set.⁶

Till here, we have characterized all probabilities of interest into the solution of certain PDEs. In the following section we will present our proposed framework for efficient calculation of such probabilities.

VI. PHYSICS-INFORMED LEARNING

In this section, we present our proposed physics-informed learning framework to efficiently solve the associating PDEs for risk probabilities of interest.

A. Physics-informed Learning Framework

For simplicity of notation, we use one single notation F to denote the probabilities of interest *i.e.*, equations (18.A), (19.A), (20.A) and (21.A), and use W_F to denote the associated PDEs (18.B), (19.B), (20.B) and (21.B). For instance, for complementary cumulative distribution of $\Phi_x(T)$ defined in (18.A), we have

$$W_F := \frac{\partial F}{\partial T} - \frac{1}{2} \nabla \cdot (D \nabla F) + \mathcal{L}_{\rho - \frac{1}{2} \nabla \cdot D} F. \quad (22)$$

While the PDE provides a way to get the actual risk probability of the system, to solve a PDE using numerical techniques is not easy in general, especially when the coefficients are time varying as in the case of (22). Monte Carlo (MC) methods provide another way to solve this problem. Assume the dynamics of the system is given, one can simulate the system for an initial condition multiple times to get an empirical estimate of the risk probability by calculating the ratio of unsafe trajectories over all trajectories. However, MC requires huge number of trajectories to get accurate estimation, and the evaluation of the risk probability can only be conducted at a single point at a time.

To leverage the advantages of PDE and MC and to overcome their drawbacks, we propose to use physics-informed neural networks (PINNs) to learn the mapping from the state and time horizon to the risk probability value F . Fig. 2 shows the architecture of the PINN. The PINN takes the state-time pair (x, T) and the system parameter λ as the input, and outputs the risk probability prediction \hat{F} , the state and time derivatives $\frac{\partial \hat{F}}{\partial x}$ and $\frac{\partial \hat{F}}{\partial T}$, and the Hessian $\frac{\partial^2 \hat{F}}{\partial x^2}$, which come naturally from the automatic differentiation in deep learning frameworks such as PyTorch [54] and TensorFlow [55]. Unlike standard PINN, we add the system parameter λ as an input to achieve adaptations on varying system parameters. Assume the PINN is parameterized by θ , the loss function is defined as

$$\mathcal{L}(\theta) = \omega_p \mathcal{L}_p(\theta) + \omega_d \mathcal{L}_d(\theta), \quad (23)$$

where

$$\begin{aligned} \mathcal{L}_p(\theta) &= \frac{1}{|\mathcal{P}|} \sum_{(x, T) \in \mathcal{P}} \|W_{\hat{F}_\theta}(x, T)\|_2^2, \\ \mathcal{L}_d(\theta) &= \frac{1}{|\mathcal{D}|} \sum_{(x, T) \in \mathcal{D}} \|\hat{F}_\theta(x, T) - \bar{F}(x, T)\|_2^2. \end{aligned} \quad (24)$$

Here, \bar{F} is the training data, \hat{F}_θ is the prediction from the PINN, \mathcal{P} and \mathcal{D} are the training point sets for the physics model and external data, respectively. The loss function \mathcal{L} consists of two parts, the physics model loss \mathcal{L}_p and data loss \mathcal{L}_d . The physics model loss \mathcal{L}_p measures the satisfaction of the PDE constraints for the learned output. It calculates the actual PDE equation value $W_{\hat{F}_\theta}$, which is supposed to be 0, and use its 2-norm as the loss. The data loss \mathcal{L}_d measures the accuracy of the prediction of PINN on the training data. It calculates the mean square error between the PINN prediction and the training data point as the loss. The overall loss function \mathcal{L} is the weighted sum of the physics model loss and data loss with weighting coefficients ω_p and ω_d . In practice, we suggest setting a larger weight ω_d when sufficient data are available, and a smaller weight otherwise. Usually one can set both coefficients ω_p and ω_d close to 1 and increase the weight ω_p or ω_d if the physics model or data is more reliable.

The resulting PIPE framework combines MC data and the governing PDE into a PINN to learn the risk probability. The advantages of the PIPE framework include fast inference at test time, accurate estimation, and ability to generalize from the combination of data and model.

B. Performance Analysis

Here we provide performance analysis of PIPE. We first show that for standard neural networks (NNs) without physics model constraints, it is fundamentally difficult to estimate the risk probability of a longer time horizon than those generated from sampled trajectories. We then show that with the PINN, we are able to estimate the risk probability at any state for any time horizon with bounded error. Let Ω be the state space, $\tau = [0, T_H]$ be the time domain, $\Sigma = (\partial\Omega \times [0, T_H]) \cup (\Omega \times \{0\})$ be the boundary of the space-time domain. Denote $D := \Omega \times \tau$ for notation simplicity and denote \bar{D} be the interior of D . All proofs can be found in the Appendix.

Corollary 1. *Suppose that $D \in \mathbb{R}^{d+1}$ is a bounded domain, $u \in C^0(\bar{D}) \cap C^2(D)$ is the solution to the PDE of interest, and $\tilde{u}(x, T), (x, T) \in \Sigma$ is the boundary condition. Let Σ_s be a strict sub-region in Σ , and D_s be a strict sub-region in D . Consider a neural network F_θ that is parameterized by θ and has sufficient representation capabilities. For $\forall M > 0$, there can exist $\bar{\theta}$ that satisfies both of the following conditions simultaneously:*

- 1) $\sup_{(x, T) \in \Sigma_s} |F_{\bar{\theta}}(x, T) - \tilde{u}(x, T)| < \delta_1$
- 2) $\sup_{(x, T) \in D_s} |F_{\bar{\theta}}(x, T) - u(x, T)| < \delta_2$

and

$$\sup_{(x, T) \in D} |F_{\bar{\theta}}(x, T) - u(x, T)| \geq M. \quad (25)$$

Theorem 5. *Suppose that $D \in \mathbb{R}^{d+1}$ is a bounded domain, $u \in C^0(\bar{D}) \cap C^2(D)$ is the solution to the PDE of interest, and*

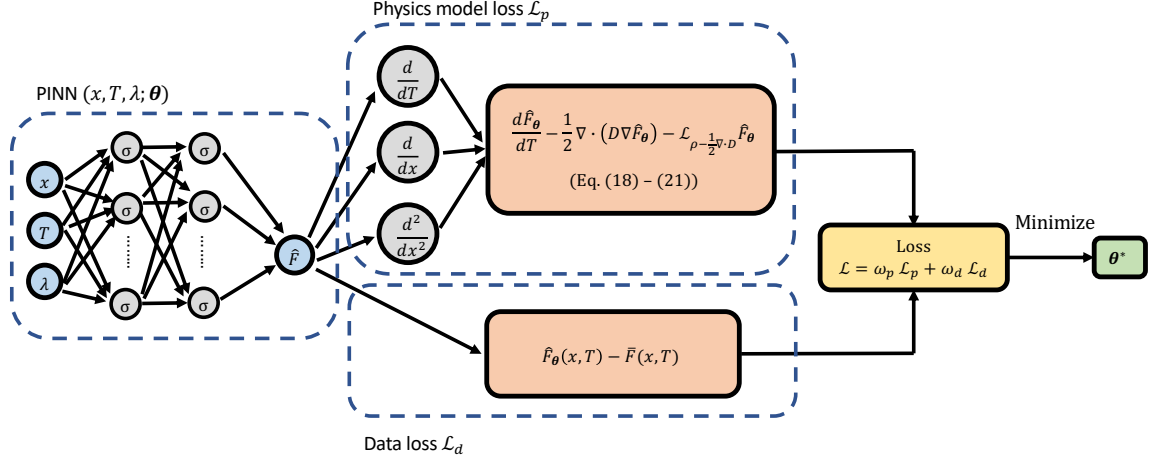


Fig. 2: The training scheme of the physics-informed neural network.

$\tilde{u}(x, T), (x, T) \in \Sigma$ is the boundary condition. Let F_θ denote a PINN parameterized by θ . If the following conditions holds:

- 1) $\mathbb{E}_{\mathbf{Y}} [|F_\theta(\mathbf{Y}) - \tilde{u}(\mathbf{Y})|] < \delta_1$, where \mathbf{Y} is uniformly sampled from Σ
- 2) $\mathbb{E}_{\mathbf{X}} [|W_{F_\theta}(\mathbf{X})|] < \delta_2$, where \mathbf{X} is uniformly sampled from D
- 3) $F_\theta, W_{F_\theta}, u$ are $\frac{1}{2}$ Lipschitz continuous on D .

Then the error of F_θ over D is bounded by

$$\sup_{(x, T) \in D} |F_\theta(x, T) - u(x, T)| \leq \tilde{\delta}_1 + C \frac{\tilde{\delta}_2}{\sigma^2} \quad (26)$$

where C is a constant depending on D, Σ and W , and

$$\tilde{\delta}_1 = \max \left\{ \frac{2\delta_1 |\Sigma|}{R_\Sigma |\Sigma|}, 2l \cdot \left(\frac{\delta_1 |\Sigma| \cdot \Gamma(d/2 + 1)}{l R_\Sigma \cdot \pi^{d/2}} \right)^{\frac{1}{d+1}} \right\},$$

$$\tilde{\delta}_2 = \max \left\{ \frac{2\delta_2 |D|}{R_D |D|}, 2l \cdot \left(\frac{\delta_2 |D| \cdot \Gamma((d+1)/2 + 1)}{l R_D \cdot \pi^{(d+1)/2}} \right)^{\frac{1}{d+2}} \right\}, \quad (27)$$

with $R_{(\cdot)}$ being the regularity of (\cdot) , $\|(\cdot)\|$ is the Lebesgue measure of a set (\cdot) and Γ is the Gamma function.

Corollary 1 says that standard NN can give arbitrarily inaccurate prediction due to insufficient physical constraints. This explains why risk estimation problems cannot be handled solely on fitting sampled data. Theorem 5 says that when the PDE constraint is imposed on the full space-time domain, the prediction of the PINN has bounded error.

Also, we present the following theorem based on [56] to show that the PINN converges to the solution of the safety-related PDE when the number of training data increases under some additional regularity assumptions.

Assumption 1. The system dynamics f, g and σ in (1) are bounded continuous functions. Also, for any $x \in \mathcal{X}$, $\text{eig}(\sigma(x)) \neq 0$ and $\sigma^{11}(x) > 0$, i.e., all eigenvalues of σ is non-zero and the first row first column entry of the noise magnitude is positive.

Assumption 2. Let $D \in \mathbb{R}^{d+1}$ and $\Gamma \in \mathbb{R}^d$ be the state-time space of interest and a subset of its boundary, respectively. Let

μ_r and μ_b be probability distributions defined on D and Γ . Let ρ_r be the probability density of μ_r with respect to $(d+1)$ -dimensional Lebesgue measure on D . Let ρ_b be the probability density of μ_b with respect to d -dimensional Hausdorff measure on Γ . We assume the following conditions.

- 1) D is at least of class $C^{0,1}$.
- 2) ρ_r and ρ_b are supported on D and Γ , respectively. Also, $\inf_D \rho_r > 0$ and $\inf_\Gamma \rho_b > 0$.
- 3) For $\epsilon > 0$, there exists partitions of D and Γ , $\{D_j^\epsilon\}_{j=1}^{K_r}$ and $\{\Gamma_j^\epsilon\}_{j=1}^{K_b}$ that depend on ϵ such that for each j , there are cubes $H_\epsilon(\mathbf{z}_{j,r})$ and $H_\epsilon(\mathbf{z}_{j,b})$ of side length ϵ centered at $\mathbf{z}_{j,r} \in D_j^\epsilon$ and $\mathbf{z}_{j,b} \in \Gamma_j^\epsilon$, respectively, satisfying $D_j^\epsilon \subset H_\epsilon(\mathbf{z}_{j,r})$ and $\Gamma_j^\epsilon \subset H_\epsilon(\mathbf{z}_{j,b})$.
- 4) There exists positive constants c_r, c_b such that $\forall \epsilon > 0$, the partitions from the above satisfy $c_r \epsilon^d \leq \mu_r(D_j^\epsilon)$ and $c_b \epsilon^{d-1} \leq \mu_b(\Gamma_j^\epsilon)$ for all j . There exists positive constants C_r, C_b such that $\forall x_r \in D$ and $\forall x_b \in \Gamma$, $\mu_r(B_\epsilon(x_r) \cap D) \leq C_r \epsilon^d$ and $\mu_b(B_\epsilon(x_b) \cap \Gamma) \leq C_b \epsilon^{d-1}$ where $B_\epsilon(x)$ is a closed ball of radius ϵ centered at x . Here C_r, c_r depend only on (D, μ_r) and C_b, c_b depend only on (Γ, μ_b) .
- 5) When $d = 1$, we assume that all boundary points are available. Thus, no random sample is needed on the boundary.
- 6) For $x' \in \partial D$, there exists a closed ball \bar{B} in \mathbb{R}^d such that $\bar{B} \cap \bar{D} = \{x'\}$.

Note that Assumption 1 is not strict for most systems⁹ and Assumption 2 is mild and can be satisfied in many practical cases (e.g., $D = (0, 1)^d$).

Theorem 6. Suppose Assumption 1 holds, and $D \in \mathbb{R}^{d+1}$ is a bounded domain that satisfies Assumption 2, $u \in C^0(\bar{D}) \cap C^2(D)$ is the solution to the PDE of interest. Let m_r be the number of training data in D . Let F_{m_r} be the physics-informed neural networks that minimize the losses (23) with m_r training data. Assume for any m_r , architecture-wise the

⁹the noise magnitude requirement can be easily satisfied by rearranging the sequence of the state if the first state has zero noise.

physics-informed neural network has enough representation power to characterize u , then

$$\lim_{m_r \rightarrow \infty} F_{m_r} = u. \quad (28)$$

Till here, we have shown error bounds and convergence properties of the PIPE framework. For approximation error of PINNs in terms of neural network sizes (number of layers and number of neurons per layer), previous works on universal approximation theorem have shown that sufficiently large PINNs can approximate PDEs uniformly [21]–[24].

VII. EXPERIMENTS

We conduct four experiments to illustrate the efficacy of the proposed method. The system dynamics of interest is (1) with $X \in \mathbb{R}$, $f(X) \equiv \lambda$, $g(X) \equiv 0$ and $\sigma(X) \equiv 1$. The system dynamics become

$$dX_t = \lambda dt + dW_t. \quad (29)$$

The safe set is defined as (3) with $\phi(x) = x - 2$. The state-time region of interest is $\Omega \times \tau = [-10, 2] \times [0, 10]$. For risk probability, we consider the recovery probability of the system from initial state $x_0 \notin \mathcal{C}$ outside the safe set. Specifically, from section V we know that the risk probability F is characterized by the solution of the following convection diffusion equation

$$\frac{\partial F}{\partial T}(x, T) = \lambda \frac{\partial F}{\partial x}(x, T) + \frac{1}{2} \text{tr} \left(\frac{\partial^2 F}{\partial x^2}(x, T) \right), \quad (30)$$

with initial condition $F(x, 0) = \mathbf{1}(x \geq 2)$ and boundary condition $F(2, T) = 1$. We choose this system because we have the analytical solution of (30) as ground truth for comparison, as given by

$$F(x, T) = \int_0^T \frac{(2-x)}{\sqrt{2\pi t^3}} \exp \left(-\frac{((2-x) - \lambda t)^2}{2t} \right) dt. \quad (31)$$

The empirical data of the risk probability is acquired by running MC with the system dynamics (1) with initial state $x = x_0$ multiple times, and calculate the number of trajectories where the state recovers to the safe set during the time horizon $[0, T]$ over the full trajectory number, *i.e.*,

$$\bar{F}(x, T) = \mathbb{P}(\exists t \in [0, T], x_t \in \mathcal{C} \mid x_0 = x) = \frac{N_{\text{recovery}}}{N}, \quad (32)$$

where N is the number of sample trajectories and is a tunable parameter that affects the accuracy of the estimated risk probability. Specifically, larger N gives more accurate estimation.

In all experiments, we use PINN with 3 hidden layers and 32 neurons per layer. The activation function is chosen as hyperbolic tangent function (tanh). We use Adam optimizer [57] for training with initial learning rate set as 0.001. The PINN parameters θ is initialized via Glorot uniform initialization. The weights in the loss function (23) are set to be $\omega_p = \omega_d = 1$. We train the PINN for 60000 epochs in all experiments. The simulation is constructed based on the DeepXDE framework [58]. Experiment details, simulation results on higher-dimensional systems, and applications to stochastic safe control can be found in the Appendix.

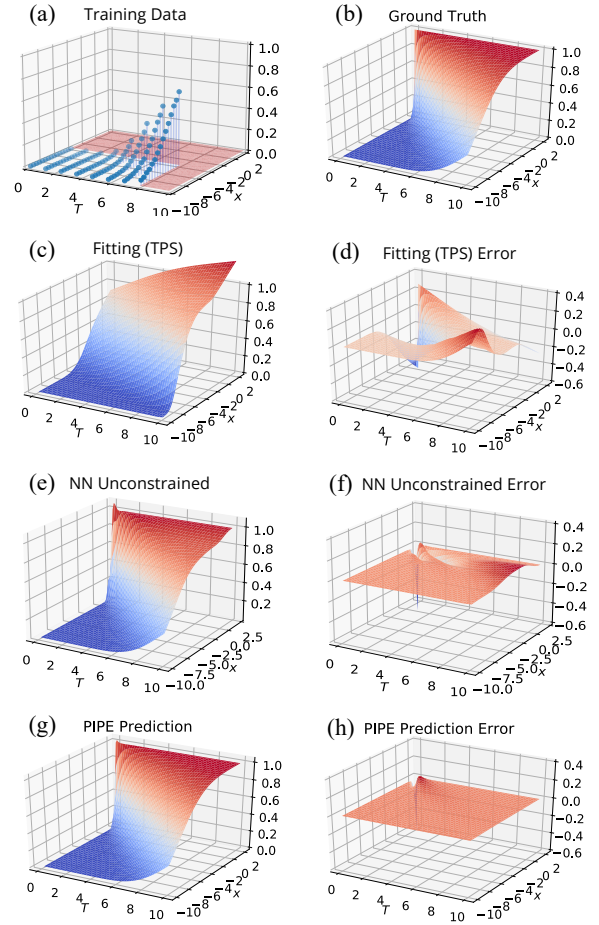


Fig. 3: Settings and results of the risk probability generalization task. Note that shaded area in (a) in the spatial-temporal space are not covered by training data. MC with fitting (TPS), neural network without PDE constraint and the proposed PIPE framework are compared. The average absolute error of prediction is 9.2×10^{-2} for TPS, and 1.5×10^{-2} for neural network without PDE constraints, 0.3×10^{-2} for PIPE.

A. Generalization to unseen regions

In this experiment, we test the generalization ability of PIPE to unseen regions of the state-time space. We consider system (29) with $\lambda = 1$. We train the PINN with data only on the sub-region of the state-time space $\Omega \times \tau = [-10, -4] \times [0, 8]$, but test the trained PINN on the full state-time region $\Omega \times \tau = [-10, 2] \times [0, 10]$. The training data is acquired through MC with sample trajectory number $N = 1000$, and is down-sampled to $dx = 0.4$ and $dT = 1$. For comparison, we consider MC with fitting and neural networks without the PDE constraint. Among all fitting methods (*e.g.*, cubic spline and polynomial fitting), thin plate spline (TPS) performs the best and is used for presentation. Fig. 3 visualizes the training data samples and shows the results. The spline fitting and the standard neural network do not include any physical model constraint, thus fail to accurately generalize to unseen regions in the state space. On the contrary, PIPE can infer the risk probability value very accurately on the whole state-time space due to its combination of data and the physics model.

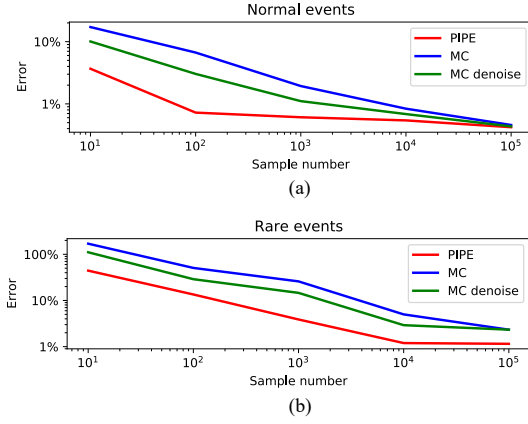


Fig. 4: Percentage error of risk probability estimation for different MC sample numbers for (a) rare events and (b) normal events. PIPE, MC and denoised MC with uniform kernel filtering are compared. Both error and sample number are in log scale.

B. Efficient estimation of risk probability

In this experiment, we show that PIPE will give more efficient estimations of risk probability in terms of accuracy and sample number compared to MC and its variants. We consider system (29) with $\lambda = 1$. The training data is sampled on the state-time space $\Omega \times \tau = [-10, 2] \times [0, 10]$ with $dx = 0.2$ and $dT = 0.1$. We compare the risk probability estimation error of PIPE and MC, on two regions in the state-time space:

- 1) Normal event region: $\Omega \times \tau = [-6, -2] \times [4, 6]$, where the average probability is 0.412.
- 2) Rare event region: $\Omega \times \tau = [-2, 0] \times [8, 10]$, where the average probability is 0.985.

For fairer comparison, we use a uniform filter of kernel size 3 on the MC data to smooth out the noise, as the main cause of inaccuracy of MC estimation is sampling noise. Fig. 4 shows the percentage errors of risk probability inference under different MC sample numbers N . As the sample number goes up, prediction errors for all three approaches decrease. The denoised MC has lower error compared to standard MC as a result of denoising, and their errors tend to converge since the sampling noise contributes less to the error as the sample number increases. On both rare events and normal events, PIPE yields more accurate estimation than MC and denoised MC across all sample numbers. This indicates that PIPE has better sample efficiency than MC and its variants, as it requires less sample data to achieve the same prediction accuracy. This desired feature of PIPE is due to the fact that it incorporates model knowledge into the MC data to further enhance its accuracy by taking the physics-informed neighboring relationships of the data into consideration.

C. Adaptation on changing system parameters

In this experiment, we show that PIPE will allow generalization to uncertain parameters of the system. We consider system (29) with varying $\lambda \in [0, 2]$. We use MC data with sample number $N = 10000$ for a fixed set of $\lambda_{\text{train}} =$

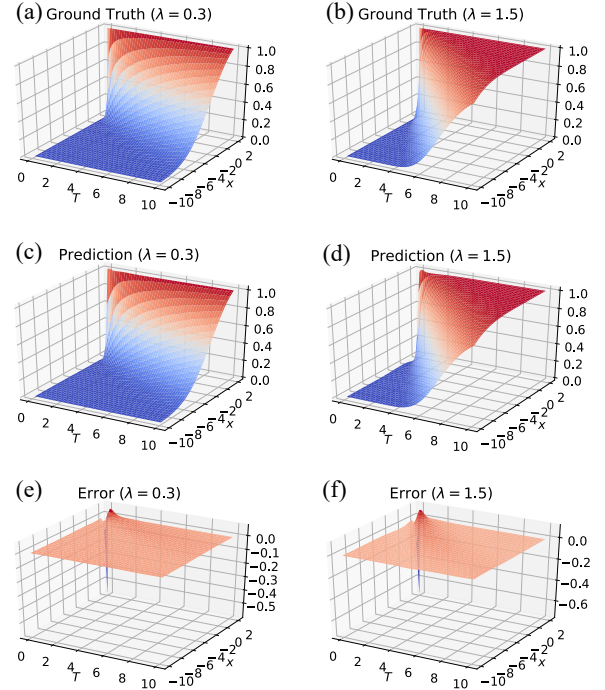


Fig. 5: Risk probability prediction of PIPE on unseen system parameters. The average absolute error of the prediction is 0.70×10^{-2} .

$[0.1, 0.5, 0.8, 1]$ for training, and test PIPE after training on $\lambda_{\text{test}} = [0.3, 0.7, 1.2, 1.5, 2]$. Fig. 5 shows the results. We can see that PIPE is able to predict risk probability for systems with unseen and even out of distribution parameters during training. In the prediction error plot, the only region that has larger prediction error is at $T = 0$ and $x \in \partial C$ on the boundary of the safe set. This is because the risk probability at this point is not well defined (it can be either 0 or 1), and this point will not be considered in a control scenario as we are always interested in long-term safety where $T \gg 0$. This adaptation feature of the PIPE framework indicates its potential use on stochastic safe control with uncertain system parameters, and it also opens the door for physics-informed learning on a family of PDEs. In general, PDEs with different parameters can have qualitatively different behaviors, so is hard to generalize. The control theory model allows us to have a sense when the PDEs are qualitatively similar with different parameters, and thus allows generalization within the qualitatively similar cases.

D. Estimating the gradient of risk probability

In this experiment, we show that PIPE is able to generate accurate gradient predictions of risk probabilities. We consider system (29) with $\lambda = 1$. Similar to the generalization task, we train the PINN with MC data of $N = 1000$ on the sub-region $\Omega \times \tau = [-10, -4] \times [0, 8]$ and test the trained PINN on the full state-time region $\Omega \times \tau = [-10, 2] \times [0, 10]$. We then take the finite difference of the risk probability with regard to the state x to calculate its gradient, for ground truth F , MC estimation \bar{F} and PIPE prediction \hat{F}_θ . Fig. 6 shows the results. It can be seen that PIPE gives much more accurate estimation

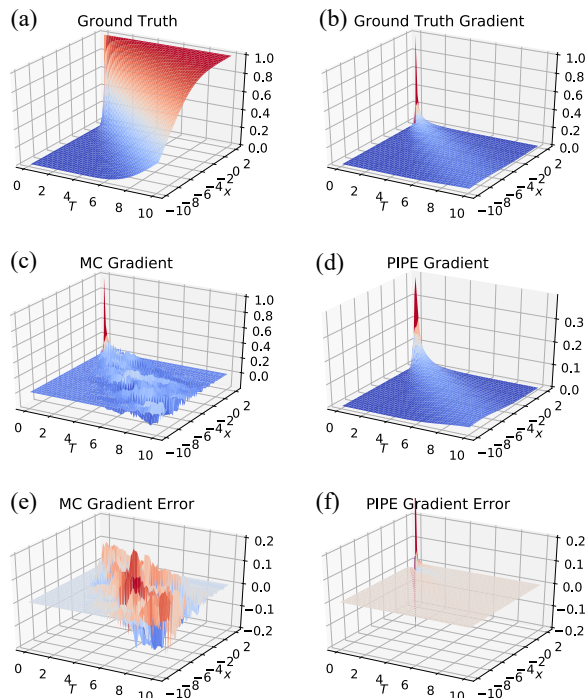


Fig. 6: Gradient of the risk probability prediction of PIPE and MC. The average absolute error of gradient prediction is 2.78×10^{-2} for MC, and 0.06×10^{-2} for PIPE.

of the risk probability gradient than MC, and this is due to the fact that PIPE incorporates physics model information inside the training process. It is also interesting that PIPE does not use any governing laws of the risk probability gradient during training, and by considering the risk probability PDE alone, it can provide very accurate estimation of the gradient. The results indicates that PIPE can enable the usage a lot of first- and higher-order stochastic safe control methods online, by providing accurate and fast estimation of the risk probability gradients.

VIII. CONCLUSION

In this paper, we characterize the exact probability distributions of the minimum and maximum barrier function values in a time interval and the first entry and exit times to and from its super level sets. The distributions of these variables are then used to characterize the probability of safety and recovery, the safety margin, and the mean and tail distributions of the failure and recovery times into the solution of certain partial differential equations (PDEs).

We further propose a physics-informed learning framework to solve the corresponding PDEs and efficiently estimate the risk probability in stochastic control systems. The framework combines data from Monte Carlo (MC) and the underlying governing PDE of the risk probability, to accurately learn the risk probability as well as its gradient. Experiments show better sample efficiencies of the physics-informed learning framework compared to MC, and the ability to generalize to unseen regions in the state space beyond training. The framework is also robust to uncertain parameters in the system

dynamics, and can infer risk probability values of a class of systems with training data only from a fixed number of systems, which provides key foundations for first- and higher-order methods for stochastic safe control.

REFERENCES

- [1] G. Rubino and B. Tuffin, *Rare event simulation using Monte Carlo methods*. John Wiley & Sons, 2009.
- [2] H. Janssen, “Monte-carlo based uncertainty analysis: Sampling efficiency and sampling convergence,” *Reliability Engineering & System Safety*, vol. 109, pp. 123–132, 2013.
- [3] F. Cérou, P. Del Moral, T. Furon, and A. Guyader, “Sequential monte carlo for rare event estimation,” *Statistics and computing*, vol. 22, no. 3, pp. 795–808, 2012.
- [4] Z. I. Botev, P. L’Ecuyer, and B. Tuffin, “Markov chain importance sampling with applications to rare event probability estimation,” *Statistics and Computing*, vol. 23, no. 2, pp. 271–285, 2013.
- [5] S.-K. Au and J. L. Beck, “Estimation of small failure probabilities in high dimensions by subset simulation,” *Probabilistic engineering mechanics*, vol. 16, no. 4, pp. 263–277, 2001.
- [6] K. Zuev, “Subset simulation method for rare event estimation: an introduction,” *arXiv preprint arXiv:1505.03506*, 2015.
- [7] A. Clark, “Control barrier functions for complete and incomplete information stochastic systems,” in *2019 American Control Conference (ACC)*. IEEE, 2019, pp. 2928–2935.
- [8] S. Prajna, A. Jadbabaie, and G. J. Pappas, “A framework for worst-case and stochastic safety verification using barrier certificates,” *IEEE Transactions on Automatic Control*, vol. 52, no. 8, pp. 1415–1428, 2007.
- [9] S. Yaghoubi, K. Majd, G. Fainekos, T. Yamaguchi, D. Prokhorov, and B. Hoxha, “Risk-bounded control using stochastic barrier functions,” *IEEE Control Systems Letters*, 2020.
- [10] C. Santoyo, M. Dutreix, and S. Coogan, “A barrier function approach to finite-time stochastic system verification and control,” *Automatica*, vol. 125, p. 109439, 2021.
- [11] R. Cheng, M. J. Khojasteh, A. D. Ames, and J. W. Burdick, “Safe multi-agent interaction through robust control barrier functions with learned uncertainties,” in *2020 59th IEEE Conference on Decision and Control (CDC)*. IEEE, 2020, pp. 777–783.
- [12] M. Raissi, P. Perdikaris, and G. E. Karniadakis, “Physics-informed neural networks: A deep learning framework for solving forward and inverse problems involving nonlinear partial differential equations,” *Journal of Computational physics*, vol. 378, pp. 686–707, 2019.
- [13] J. Han, A. Jentzen, and W. E., “Solving high-dimensional partial differential equations using deep learning,” *Proceedings of the National Academy of Sciences*, vol. 115, no. 34, pp. 8505–8510, 2018.
- [14] S. Cuomo, V. S. Di Cola, F. Giampaolo, G. Rozza, M. Raissi, and F. Piccialli, “Scientific machine learning through physics-informed neural networks: Where we are and what’s next,” *Journal of Scientific Computing*, vol. 92, no. 3, p. 88, 2022.
- [15] G. S. Misyris, A. Venzke, and S. Chatzivasileiadis, “Physics-informed neural networks for power systems,” in *2020 IEEE Power & Energy Society General Meeting (PESGM)*. IEEE, 2020, pp. 1–5.
- [16] S. Cai, Z. Mao, Z. Wang, M. Yin, and G. E. Karniadakis, “Physics-informed neural networks (pinns) for fluid mechanics: A review,” *Acta Mechanica Sinica*, pp. 1–12, 2022.
- [17] F. Sahli Costabal, Y. Yang, P. Perdikaris, D. E. Hurtado, and E. Kuhl, “Physics-informed neural networks for cardiac activation mapping,” *Frontiers in Physics*, vol. 8, p. 42, 2020.
- [18] L. Yang, X. Meng, and G. E. Karniadakis, “B-pinns: Bayesian physics-informed neural networks for forward and inverse pde problems with noisy data,” *Journal of Computational Physics*, vol. 425, p. 109913, 2021.
- [19] L. Lu, R. Pestourie, W. Yao, Z. Wang, F. Verdugo, and S. G. Johnson, “Physics-informed neural networks with hard constraints for inverse design,” *SIAM Journal on Scientific Computing*, vol. 43, no. 6, pp. B1105–B1132, 2021.
- [20] K. Shukla, A. D. Jagtap, and G. E. Karniadakis, “Parallel physics-informed neural networks via domain decomposition,” *Journal of Computational Physics*, vol. 447, p. 110683, 2021.
- [21] J. Sirignano and K. Spiliopoulos, “Dgm: A deep learning algorithm for solving partial differential equations,” *Journal of computational physics*, vol. 375, pp. 1339–1364, 2018.

- [22] P. Grohs, F. Hornung, A. Jentzen, and P. Von Wurstemberger, *A proof that artificial neural networks overcome the curse of dimensionality in the numerical approximation of Black–Scholes partial differential equations*. American Mathematical Society, 2023, vol. 284, no. 1410.
- [23] J. Darbon, G. P. Langlois, and T. Meng, “Overcoming the curse of dimensionality for some hamilton–jacobi partial differential equations via neural network architectures,” *Research in the Mathematical Sciences*, vol. 7, no. 3, p. 20, 2020.
- [24] J. Darbon and T. Meng, “On some neural network architectures that can represent viscosity solutions of certain high dimensional hamilton–jacobi partial differential equations,” *Journal of Computational Physics*, vol. 425, p. 109907, 2021.
- [25] T. De Ryck and S. Mishra, “Error analysis for physics-informed neural networks (pinns) approximating kolmogorov pdes,” *Advances in Computational Mathematics*, vol. 48, no. 6, p. 79, 2022.
- [26] S. Mishra and R. Molinaro, “Estimates on the generalization error of physics-informed neural networks for approximating pdes,” *IMA Journal of Numerical Analysis*, vol. 43, no. 1, pp. 1–43, 2023.
- [27] —, “Estimates on the generalization error of physics-informed neural networks for approximating a class of inverse problems for pdes,” *IMA Journal of Numerical Analysis*, vol. 42, no. 2, pp. 981–1022, 2022.
- [28] Y. Qian, Y. Zhang, Y. Huang, and S. Dong, “Physics-informed neural networks for approximating dynamic (hyperbolic) pdes of second order in time: Error analysis and algorithms,” *Journal of Computational Physics*, vol. 495, p. 112527, 2023.
- [29] Z. Fang, “A high-efficient hybrid physics-informed neural networks based on convolutional neural network,” *IEEE Transactions on Neural Networks and Learning Systems*, vol. 33, no. 10, pp. 5514–5526, 2021.
- [30] G. Pang, L. Lu, and G. E. Karniadakis, “fpinns: Fractional physics-informed neural networks,” *SIAM Journal on Scientific Computing*, vol. 41, no. 4, pp. A2603–A2626, 2019.
- [31] Y. Jiao, Y. Lai, D. Li, X. Lu, F. Wang, Y. Wang, and J. Z. Yang, “A rate of convergence of physics informed neural networks for the linear second order elliptic pdes,” *arXiv preprint arXiv:2109.01780*, 2021.
- [32] M. Pereira, Z. Wang, I. Exarchos, and E. Theodorou, “Safe optimal control using stochastic barrier functions and deep forward-backward sdes,” in *Conference on Robot Learning*. PMLR, 2021, pp. 1783–1801.
- [33] S. Chaudhari, S. Pranav, and J. M. Moura, “Learning gradients of convex functions with monotone gradient networks,” in *ICASSP 2023-2023 IEEE International Conference on Acoustics, Speech and Signal Processing (ICASSP)*. IEEE, 2023, pp. 1–5.
- [34] D. E. Rumelhart, G. E. Hinton, and R. J. Williams, “Learning representations by back-propagating errors,” *nature*, vol. 323, no. 6088, pp. 533–536, 1986.
- [35] J. Lee and G. AlRegib, “Gradients as a measure of uncertainty in neural networks,” in *2020 IEEE International Conference on Image Processing (ICIP)*. IEEE, 2020, pp. 2416–2420.
- [36] V. Sitzmann, J. Martel, A. Bergman, D. Lindell, and G. Wetzstein, “Implicit neural representations with periodic activation functions,” *Advances in neural information processing systems*, vol. 33, pp. 7462–7473, 2020.
- [37] D. Xu, P. Wang, Y. Jiang, Z. Fan, and Z. Wang, “Signal processing for implicit neural representations,” *Advances in Neural Information Processing Systems*, vol. 35, pp. 13 404–13 418, 2022.
- [38] Y. K. Nakka, A. Liu, G. Shi, A. Anandkumar, Y. Yue, and S.-J. Chung, “Chance-constrained trajectory optimization for safe exploration and learning of nonlinear systems,” *IEEE Robotics and Automation Letters*, vol. 6, no. 2, pp. 389–396, 2020.
- [39] H. Zhu and J. Alonso-Mora, “Chance-constrained collision avoidance for mavs in dynamic environments,” *IEEE Robotics and Automation Letters*, vol. 4, no. 2, pp. 776–783, 2019.
- [40] S. Pfrommer, T. Gautam, A. Zhou, and S. Sojoudi, “Safe reinforcement learning with chance-constrained model predictive control,” in *Learning for Dynamics and Control Conference*. PMLR, 2022, pp. 291–303.
- [41] Z. Wang, H. Jing, C. Kurniawan, A. Chern, and Y. Nakahira, “Myopically verifiable probabilistic certificate for long-term safety,” *arXiv preprint arXiv:2110.13380*, 2021.
- [42] S. Gu, L. Yang, Y. Du, G. Chen, F. Walter, J. Wang, Y. Yang, and A. Knoll, “A review of safe reinforcement learning: Methods, theory and applications,” *arXiv preprint arXiv:2205.10330*, 2022.
- [43] J. Garcia and F. Fernández, “A comprehensive survey on safe reinforcement learning,” *Journal of Machine Learning Research*, vol. 16, no. 1, pp. 1437–1480, 2015.
- [44] Z. Wang, H. Jing, C. Kurniawan, A. Chern, and Y. Nakahira, “Myopically verifiable probabilistic certificates for safe control and learning,” *arXiv preprint arXiv:2404.16883*, 2024.
- [45] Y. Liu, A. Halev, and X. Liu, “Policy learning with constraints in model-free reinforcement learning: A survey,” in *The 30th International Joint Conference on Artificial Intelligence (IJCAI)*, 2021.
- [46] S. Xu and M. Zhu, “Online constrained meta-learning: Provable guarantees for generalization,” in *Thirty-seventh Conference on Neural Information Processing Systems*, 2023.
- [47] B. Øksendal, *Stochastic Differential Equations: An Introduction with Applications*, 6th ed., ser. Universitext. Berlin Heidelberg: Springer-Verlag, 2003.
- [48] A. N. Borodin, *Stochastic processes*. Springer, 2017.
- [49] S. Lefèvre, D. Vasquez, and C. Laugier, “A survey on motion prediction and risk assessment for intelligent vehicles,” *ROBOMECH journal*, vol. 1, no. 1, pp. 1–14, 2014.
- [50] D. Ferguson, M. Darms, C. Urmson, and S. Kolski, “Detection, prediction, and avoidance of dynamic obstacles in urban environments,” in *2008 IEEE Intelligent Vehicles Symposium*, 2008, pp. 1149–1154.
- [51] A. Agrawal and K. Sreenath, “Discrete control barrier functions for safety-critical control of discrete systems with application to bipedal robot navigation,” in *Robotics: Science and Systems*, 2017.
- [52] H. Khali, “Adaptive output feedback control of nonlinear systems,” *IEEE Transactions on Automatic Control*, vol. 41, pp. 177–188, 1996.
- [53] H. J. Kushner, “Stochastic stability and control,” Brown Univ Providence RI, Tech. Rep., 1967.
- [54] A. Paszke, S. Gross, F. Massa, A. Lerer, J. Bradbury, G. Chanan, T. Killeen, Z. Lin, N. Gimelshein, L. Antiga *et al.*, “Pytorch: An imperative style, high-performance deep learning library,” *Advances in neural information processing systems*, vol. 32, 2019.
- [55] M. Abadi, A. Agarwal, P. Barham, E. Brevdo, Z. Chen, C. Citro, G. S. Corrado, A. Davis, J. Dean, M. Devin *et al.*, “Tensorflow: Large-scale machine learning on heterogeneous distributed systems,” *arXiv preprint arXiv:1603.04467*, 2016.
- [56] Y. Shin, J. Darbon, and G. E. Karniadakis, “On the convergence of physics informed neural networks for linear second-order elliptic and parabolic type pdes,” *arXiv preprint arXiv:2004.01806*, 2020.
- [57] D. P. Kingma and J. Ba, “Adam: A method for stochastic optimization,” *arXiv preprint arXiv:1412.6980*, 2014.
- [58] L. Lu, X. Meng, Z. Mao, and G. E. Karniadakis, “Deepxde: A deep learning library for solving differential equations,” *SIAM Review*, vol. 63, no. 1, pp. 208–228, 2021.
- [59] H. Pham, *Continuous-time stochastic control and optimization with financial applications*. Springer Science & Business Media, 2009, vol. 61.
- [60] G. Cybenko, “Approximation by superpositions of a sigmoidal function,” *Mathematics of control, signals and systems*, vol. 2, no. 4, pp. 303–314, 1989.
- [61] W. Peng, W. Zhou, J. Zhang, and W. Yao, “Accelerating physics-informed neural network training with prior dictionaries,” *arXiv preprint arXiv:2004.08151*, 2020.
- [62] D. Gilbarg, N. S. Trudinger, D. Gilbarg, and N. Trudinger, *Elliptic partial differential equations of second order*. Springer, 1977, vol. 224, no. 2.
- [63] W. S. Cleveland, “Lowess: A program for smoothing scatterplots by robust locally weighted regression,” *American Statistician*, vol. 35, no. 1, p. 54, 1981.

APPENDIX

A. Proof of Theorem 1 and Theorem 3

The proof of Theorem 1 and Theorem 3 is based on the lemmas presented below. These lemmas relate the distributions of various functionals of a diffusion process $X_t \in \mathbb{R}^n, t \in \mathbb{R}_+$ with deterministic convection-diffusion equations. Let $X_t \in \mathbb{R}^n, t \in \mathbb{R}_+$ be a solution of the SDE

$$dX_t = \mu(X_t)dt + \sigma(X_t)dW_t, \quad (33)$$

We assume sufficient regularity in the coefficients of (33) such that (33) has a unique solution.¹

We first present a variant of the Feynman–Kac Representation [59, Theorem 1.3.17].

Lemma 1 (Feynman–Kac Representation). *Consider the diffusion process (33) with $X_0 = x \in \mathbb{R}^n$. Let $V : \mathbb{R}^n \times \mathbb{R}_+ \rightarrow \mathbb{R}$, $\beta : \mathbb{R}^n \times \mathbb{R}_+ \rightarrow \mathbb{R}$ and $\psi : \mathbb{R}^n \rightarrow \mathbb{R}$ be some given functions. The solution of the Cauchy problem*

$$\begin{cases} \frac{\partial U}{\partial T} = \frac{1}{2} \text{tr}(\sigma\sigma^\top \text{Hess } U) + \mathcal{L}_\mu U - VU + \beta, & T > 0, \\ U(x, 0) = \psi(x) \end{cases} \quad (34)$$

is given by

$$\begin{aligned} U(x, T) = \mathbb{E}_x \left[e^{-\int_0^T V(X_t, T-t) dt} \psi(X_T) \right. \\ \left. + \int_0^T e^{-\int_0^\tau V(X_t, T-t) dt} \beta(X_\tau, T-\tau) d\tau \right]. \end{aligned} \quad (35)$$

While the original statement given in [59, Theorem 1.3.17] presents U as a function of t that moves backward in time, we present U as a function of T that moves forward in time. Even though both approaches express the time derivative with opposite signs, both yield the same probability. The representation in Lemma 1 can be used to derive the following result.

Lemma 2. *Let $\mathcal{M} \subset \mathbb{R}^n$ be a domain. Consider the diffusion process (33) with the initial condition $X_0 = x \in \mathbb{R}^n$. Then the function $U : \mathbb{R}^n \times [0, \infty) \rightarrow \mathbb{R}$ defined by*

$$U(x, T) := \mathbb{P}_x(X_t \in \mathcal{M}, \forall t \in [0, T]) \quad (36)$$

is the solution to the convection-diffusion equation

$$\begin{cases} \frac{\partial U}{\partial T} = \frac{1}{2} \text{tr}(\sigma\sigma^\top \text{Hess } U) + \mathcal{L}_\mu U, & x \in \mathcal{M}, T > 0, \\ U(x, T) = 0, & x \notin \mathcal{M}, T > 0, \\ U(x, 0) = \mathbb{1}_{\mathcal{M}}(x), & x \in \mathbb{R}^n. \end{cases} \quad (37)$$

Proof. Applying Lemma 1 with

$$\beta(x, t) \equiv 0, \quad \psi(x) = \mathbb{1}_{\mathcal{M}}(x), \quad V(x, t) = \gamma \mathbb{1}_{\mathcal{M}^c}(x),$$

we have

$$U(x, T) = \mathbb{E}_x \left[e^{-\int_0^T \gamma \mathbb{1}_{\mathcal{M}^c}(X_t) dt} \psi(X_T) \right]. \quad (38)$$

and

$$\begin{cases} \frac{\partial U}{\partial T} = \frac{1}{2} \text{tr}(\sigma\sigma^\top \text{Hess } U) + \mathcal{L}_\mu U, & x \in \mathcal{M}, T > 0, \\ \frac{\partial U}{\partial T} = \frac{1}{2} \text{tr}(\sigma\sigma^\top \text{Hess } U) + \mathcal{L}_\mu U - \gamma U, & x \notin \mathcal{M}, T > 0, \\ U(x, 0) = \mathbb{1}_{\mathcal{M}}(x), & x \in \mathbb{R}^n. \end{cases} \quad (39)$$

Now, we take the limit of $\gamma \rightarrow \infty$. Since

$$\lim_{\gamma \rightarrow \infty} e^{-\int_0^T \gamma \mathbb{1}_{\mathcal{M}^c}(X_t) dt} = \begin{cases} 0, & \text{if } X_t \notin \mathcal{M}, \exists t \in [0, T], \\ 1, & \text{otherwise.} \end{cases},$$

(38) becomes

$$U(x, T) = \mathbb{E}_x[\mathbb{1}_{\{X_t \in \mathcal{M}, \forall t \in [0, T]\}}] \quad (40)$$

$$= \mathbb{P}_x(X_t \in \mathcal{M}, \forall t \in [0, T]). \quad (41)$$

Meanwhile, under the limit of $\gamma \rightarrow \infty$, the part of (39) with $x \notin \mathcal{M}$ and $T > 0$ reduces to the algebraic condition

$$U(x, T) = 0, \quad x \notin \mathcal{M}, T > 0. \quad (42)$$

Combining (39), (40), and (42) and gives Lemma 2. ■

Using Lemma 2, we can prove Theorem 1 and Theorem 3 as follows.

Proof. (Theorem 1) Consider the augmented space $Z_t = [\phi(X_t), X_t^\top]^\top \in \mathbb{R}^{n+1}$. The stochastic process Z_t is the solution to (16) with parameters ρ and ζ defined in (17) with the initial state

$$Z_0 = z = [\phi(x), x^\top]^\top. \quad (43)$$

Let us define

$$\mathcal{M} = \{z \in \mathbb{R}^{n+1} : z[1] \geq \ell\}. \quad (44)$$

From Lemma 2,

$$F(x, T; \ell) = \mathbb{P}_x(z_t \in \mathcal{M}, \forall t \in [0, T])$$

is the solution to the convection-diffusion equation

$$\begin{cases} \frac{\partial F}{\partial T} = \frac{1}{2} \text{tr}(\zeta \zeta^\top \text{Hess } F) + \mathcal{L}_\rho F, & z \in \mathcal{M}, T > 0, \\ F(z, T) = 0, & z \notin \mathcal{M}, T > 0, \\ F(z, 0) = \mathbb{1}_{\mathcal{M}}(z), & z \in \mathbb{R}^{n+1}. \end{cases} \quad (45)$$

To obtain (18.B), define $D = \zeta \zeta^\top$ and apply the vector identity¹⁰

$$\nabla \cdot (D \nabla F) = \mathcal{L}_{\nabla \cdot D} F + \text{tr}(D \text{Hess } F). \quad (46)$$

Proof. (Theorem 3) Consider the augmented space of $Z_t = [\phi(X_t), X_t^\top]^\top \in \mathbb{R}^{n+1}$ in (14). The stochastic process Z_t is a solution of (16) with parameters ρ and ζ defined in (17) with the initial state

$$Z_0 = z = [\phi(x), x^\top]^\top. \quad (47)$$

Let us define

$$\mathcal{M} = \{z \in \mathbb{R}^{n+1} : z[1] < \ell\}. \quad (48)$$

The CDF of $\Theta_x(T)$ is given by

$$\mathbb{P}(\Theta_x(T) < \ell) = \mathbb{P}_x(\forall t \in [0, T], \phi(X_t) < \ell) \quad (49)$$

$$= \mathbb{P}_x(\forall t \in [0, T], Z_t \in \mathcal{M}), \quad (50)$$

which, by Lemma 2, is the solution to the convection-diffusion equation (37), yielding (20.B) after the application of identity (46). ■

B. Proof of Theorem 2 and Theorem 4

The proof of Theorem 2 and Theorem 4 requires Lemma 3 and Lemma 4. We will first present these lemmas and then prove Theorem 2 and Theorem 4.

Lemma 3. Consider the diffusion process (33) with the initial point $X_0 = x$. Define the escape time as (66). Let $\psi(x), V(x)$ be continuous functions and V be non-negative. If $U : \mathbb{R}^n \rightarrow \mathbb{R}$ is the bounded solution to the boundary value problem

$$\begin{cases} \frac{1}{2} \text{tr}(\sigma \sigma^\top \text{Hess } U) + \mathcal{L}_\mu U - VU = 0, & x \in \mathcal{M}, \\ U(x) = \psi(x), & x \notin \mathcal{M}, \end{cases} \quad (51)$$

then

$$U(x) = \mathbb{E}_x \left[\psi(X_{H_{\mathcal{M}}}) e^{-\int_0^{H_{\mathcal{M}}} V(X_s) ds} \right]. \quad (52)$$

Proof. We first define a mapping $\eta : \mathbb{R} \rightarrow \mathbb{R}$ by

$$\eta(s) := U(X_s) e^{-\int_0^s V(X_v) dv}. \quad (53)$$

¹⁰The identity is a direct consequence of the Leibniz rule $\partial_i(D_{ij}\partial_j F) = (\partial_i D_{ij})\partial_j F + D_{ij}\partial_i\partial_j F$.

It satisfies

$$\eta(q) = \int_0^q d\eta(s) + \eta(0) \quad (54)$$

$$\begin{aligned} &= \int_0^q e^{-\int_0^s V(X_v) dv} [-V(X_s)U(X_s) + \mathcal{L}_\mu U(X_s) \\ &\quad + \frac{1}{2} \text{tr}(\sigma(X_s)\sigma^\top(X_s) \text{Hess } U(X_s))] ds \end{aligned} \quad (55)$$

$$\begin{aligned} &+ \int_0^q e^{-\int_0^s V(X_v) dv} \mathcal{L}_\sigma U(X_s) dW_s + \eta(0) \\ &= \int_0^q e^{-\int_0^s V(X_v) dv} \mathcal{L}_\sigma U(X_s) dW_s + \eta(0), \end{aligned} \quad (56)$$

where (55) is from Itô's Lemma; (56) is from (51) with $x \in \mathcal{M}$. Thus, its expectation satisfies

$$\mathbb{E}_x[\eta(q)] = \mathbb{E}_x[\eta(0)] \quad (57)$$

$$= \mathbb{E}_x[U(X_0)] \quad (58)$$

$$= U(x). \quad (59)$$

where (57) holds because the right hand side of (56) has zero mean; (58) is due to (53); and (59) is from the assumption that $X_0 = x$.

Next, we set

$$q = H_{\mathcal{M}}. \quad (60)$$

As (60) implies $X_q \notin \mathcal{M}$, condition (51) with $x \notin \mathcal{M}$ yields

$$U(X_q) = \psi(X_q). \quad (61)$$

Finally, we have

$$U(x) = \mathbb{E}_x[\eta(q)] \quad (62)$$

$$= \mathbb{E}_x \left[U(X_q) e^{-\int_0^q V(X_v) dv} \right] \quad (63)$$

$$= \mathbb{E}_x \left[\psi(X_q) e^{-\int_0^q V(X_v) dv} \right] \quad (64)$$

$$= \mathbb{E}_x \left[\psi(X_{H_{\mathcal{M}}}) e^{-\int_0^{H_{\mathcal{M}}} V(X_v) dv} \right], \quad (65)$$

where (62) is due to (59); (63) is due to (53); (64) is due to (61), and (65) is due to (60). ■

Lemma 4. Consider the diffusion process (33) with the initial condition $X_0 = x \in \mathbb{R}^n$. Define the escape time,

$$H_{\mathcal{M}} := \inf\{t \in \mathbb{R}_+ : X_t \notin \mathcal{M}\}. \quad (66)$$

The CDF of the escape time

$$U(x, t) = \mathbb{P}_x(H_{\mathcal{M}} \leq t), \quad t > 0, \quad (67)$$

is the solution to

$$\begin{cases} \frac{\partial U}{\partial t}(x, t) = \frac{1}{2} \text{tr}(\sigma\sigma^\top \text{Hess } U) + \mathcal{L}_\mu U, & x \in \mathcal{M}, t > 0, \\ U(x, t) = 1, & x \notin \mathcal{M}, t > 0, \\ U(x, 0) = \mathbb{1}_{\mathcal{M}^c}(x), & x \in \mathbb{R}^n. \end{cases} \quad (68)$$

Proof. Let $\gamma \in \mathbb{C}$ be a spectral parameter with $\text{Re}(\gamma) > 0$. For each fixed γ , let $\hat{U}(\cdot, \gamma) : \mathbb{R}^n \rightarrow \mathbb{C}$ be the solution of

$$\begin{cases} \frac{1}{2} \text{tr}(\sigma\sigma^\top \text{Hess } \hat{U}) + \mathcal{L}_\mu \hat{U} - \gamma \hat{V} \hat{U} = 0, & x \in \mathcal{M}, \\ \hat{U}(x, \gamma) = \hat{\psi}(x, \gamma), & x \notin \mathcal{M}. \end{cases} \quad (69)$$

According to Lemma 3, $\hat{U}(x, \gamma)$ is given by

$$\hat{U}(x, \gamma) = \mathbb{E}_x \left[\hat{\psi}(X_{H_{\mathcal{M}}}) e^{-\gamma \int_0^{H_{\mathcal{M}}} \hat{V}(X_s) ds} \right], \quad (70)$$

where X_s is the diffusion process in (33). Now, take

$$\hat{\psi}(x, \gamma) = 1/\gamma, \quad \hat{V}(x) = 1, \quad (71)$$

in (69) and (70). Then, (69) becomes

$$\begin{cases} \frac{1}{2} \text{tr}(\sigma\sigma^\top \text{Hess } \hat{U}) + \mathcal{L}_\mu \hat{U} - \gamma \hat{U} = 0, & x \in \mathcal{M}, \\ \hat{U}(x, \gamma) = 1/\gamma, & x \notin \mathcal{M}, \end{cases} \quad (72)$$

and (70) becomes

$$\begin{aligned} \hat{U}(x, \gamma) &= \mathbb{E}_x \left[\frac{1}{\gamma} e^{-\gamma H_{\mathcal{M}}} \right] \\ &= \int_0^\infty \frac{1}{\gamma} e^{-\gamma t} p_{H_{\mathcal{M}}|X_0}(t | x) dt \\ &= \int_0^\infty e^{-\gamma t} \mathbb{P}_x(H_{\mathcal{M}} \leq t) dt \end{aligned} \quad (73)$$

where integration by parts is used in (73). Here, $p_{H_{\mathcal{M}}|X_0}(t|x) = \frac{d}{dt} \mathbb{P}_x(H_{\mathcal{M}} \leq t)$ denotes the probability density function of $H_{\mathcal{M}}$ conditioned on $X_0 = x$.

Now, for fixed x , let $U(x, t)$ be the inverse Laplace transformation of $\hat{U}(x, \gamma)$. In other words,

$$\hat{U}(x, \gamma) = \int_0^\infty U(x, t) e^{-\gamma t} dt. \quad (74)$$

On one hand, comparing (73) and (74) gives

$$U(x, t) = \mathbb{P}_x(H_{\mathcal{M}} \leq t). \quad (75)$$

On the other hand, taking the inverse Laplace transformation of the PDE (72) for \hat{U} yields the PDE satisfied by U :

$$\begin{cases} \frac{\partial U}{\partial t}(x, t) = \frac{1}{2} \text{tr}(\sigma\sigma^\top \text{Hess } U) + \mathcal{L}_\mu U, & x \in \mathcal{M}, t > 0, \\ U(x, t) = 1, & x \notin \mathcal{M}, t > 0, \\ U(x, 0) = \mathbb{1}_{\mathcal{M}^c}(x), & x \in \mathbb{R}^n. \end{cases} \quad (76)$$

■

Now, we are ready to prove Theorem 2 and Theorem 4.

Proof. (Theorem 2) Let the augmented state Z_t be the solution of (16) with the initial state $Z_0 = z = [\phi(x), x^\top]^\top \in \mathbb{R}^{n+1}$. Let

$$\mathcal{M} = \{z \in \mathbb{R}^{n+1} : z[1] \geq \ell\}. \quad (77)$$

Thus, we have $\Gamma_x(\ell) = H_{\mathcal{M}}$, for G be the solution of the convection-diffusion equation with $D = \zeta\zeta^\top$

$$\begin{cases} \frac{\partial G}{\partial t} = \frac{1}{2} \nabla \cdot (D \nabla G) + \mathcal{L}_{\rho - \frac{1}{2} \nabla \cdot D} G, & z \in \mathcal{M}, t > 0, \\ G(z, t) = 1, & z \notin \mathcal{M}, t > 0, \\ G(z, 0) = \mathbb{1}_{\mathcal{M}^c}(z), & z \in \mathbb{R}^{n+1}, \end{cases}$$

which is equivalent to (19.B). From Lemma 4, we have $G(z, t; \ell) = \mathbb{P}(\Gamma_x(\ell) \leq t)$. ■

Proof. (Theorem 4) Let the augmented state space Z_t be the solution of (16) with the initial state $Z_0 = z = [\phi(x), x^\top]^\top \in \mathbb{R}^{n+1}$. Let

$$\mathcal{M} = \{z \in \mathbb{R}^{n+1} : z[1] < \ell\}. \quad (78)$$

We have $\Psi_x(\ell) = H_{\mathcal{M}}$ for N be the solution of the convection diffusion equation with $D = \zeta\zeta^\top$

$$\begin{cases} \frac{\partial N}{\partial t}(z, t) = \frac{1}{2} \nabla \cdot (D \nabla N) + \mathcal{L}_{\rho - \frac{1}{2} \nabla \cdot D} N, & z \in \mathcal{M}, t > 0, \\ N(x, t) = 1, & z \notin \mathcal{M}, t > 0, \\ N(x, 0) = \mathbb{1}_{\mathcal{M}^c}(z), & z \in \mathbb{R}^{n+1}, \end{cases}$$

which is equivalent to (21.B). From Lemma 4, we have $N(z, T; \ell) = \mathbb{P}(\Psi_x(\ell) \leq T)$. ■

C. Proof of Theorems for Physics-informed Learning

Proof. (Corollary 1) We know that u is the solution to the PDE of interest. We can construct \bar{u} such that

$$\bar{u} = \begin{cases} u, & (x, T) \in D_s \\ u + \frac{d}{d_{\max}}(M + \delta), & (x, T) \in \Omega \times \tau \setminus D_s \end{cases} \quad (79)$$

where d characterizes the distance between $(x, t) \in \Omega \setminus D_s$ and set D_s , $d_{\max} = \max_{(x,t) \in \Omega \setminus D_s} d$ is the maximum distance, and $0 < \delta < \min\{\delta_1, \delta_2\}$ is a constant. Then we have

$$\sup_{(x,T) \in \Omega \times \tau} |\bar{u}(x, t) - u(x, t)| = M + \delta \quad (80)$$

Since we assume the neural network has sufficient representation power, by universal approximation theorem [60], for δ given above, there exist $\bar{\theta}$ such that

$$\sup_{(x,T) \in \Omega \times \tau} |F_{\bar{\theta}}(x, t) - \bar{u}(x, t)| \leq \delta. \quad (81)$$

Then we have $\bar{\theta}$ satisfies

$$\begin{aligned} \sup_{(x,T) \in \Sigma_s} |F_{\bar{\theta}}(x, T) - \tilde{u}(x, T)| &< \delta_1, \\ \sup_{(x,T) \in D_s} |F_{\bar{\theta}}(x, T) - u(x, T)| &< \delta_2, \end{aligned} \quad (82)$$

and

$$\sup_{(x,T) \in \Omega \times \tau} |F_{\bar{\theta}}(x, t) - u(x, t)| \geq M. \quad (83)$$

■

The proof of Theorem 5 is based on [61], [62] by adapting the results on elliptic PDEs to parabolic PDEs. We first give some supporting definitions and lemmas. We define the second order parabolic operator L w.r.t. u as follows.

$$\begin{aligned} L[u] := & -\frac{\partial u}{\partial T} + \sum_{i,j} a_{i,j}(x, T) \frac{\partial^2 u}{\partial x_i \partial x_j} \\ & + \sum_i b_i(x, T) \frac{\partial u}{\partial x_i} + c(x, T)u. \end{aligned} \quad (84)$$

Let $A(x) := [a_{i,j}(x, T)]_{i,j} \in \mathbb{R}^{d \times d}$ and $b(x, T) := [b_i(x)]_i \in \mathbb{R}^d$. We consider uniform parabolic operators, where A is positive definite, with the smallest eigenvalue $\lambda > 0$.

Let $\Omega \times \tau \in \mathbb{R}^{d+1}$ be a bounded domain of interest, where Σ is the boundary of $\Omega \times \tau$. We consider the following partial differential equation for the function $u(\cdot)$.

$$\begin{aligned} L[u](x, T) &= q(x, T), & (x, T) \in \Omega \times \tau \\ u(x, T) &= \tilde{u}(x, T), & (x, T) \in \Sigma \end{aligned} \quad (85)$$

We know that the risk probability PDEs (18)-(21) are parabolic PDEs and can be written in the form of (85). Specifically, in our case we have $c(x, T) \equiv 0$ and $A = \frac{1}{2}\sigma^2 I$ which gives $\lambda = \frac{1}{2}\sigma^2$.

For any space $\Omega \in \mathbb{R}^d$, for any function $f : \mathbb{R}^d \rightarrow \mathbb{R}$, we define the L_1 norm of the function f on Ω to be

$$\|f\|_{L_1(\Omega)} := \int_{\Omega} f(\mathbf{X}) d\mathbf{X}. \quad (86)$$

With this definition, we know that

$$\mathbb{E}_{\mathbf{X}} [f] = \|f\|_{L_1(\Omega)} / |\Omega|, \quad (87)$$

where \mathbf{X} is uniformly sampled from Ω , and $|\Omega|$ denote the size of the space Ω .

Corollary 2. Weak maximum principle. Suppose that $D = \Omega \times \tau$ is bounded, L is uniformly parabolic with $c \leq 0$ and that $u \in C^0(\bar{D}) \cap C^2(D)$ satisfies $Lu \geq 0$ in D , and $M = \max_{\bar{D}} u \geq 0$. Then

$$\max_{\bar{D}} u = \max_{\Sigma} u. \quad (88)$$

Corollary 3. Comparison principle. Suppose that D is bounded and L is uniformly parabolic. If $u, v \in C^0(\bar{D}) \cap C^2(D)$ satisfies $Lu \leq Lv$ in D and $u \geq v$ on Σ , then $u \geq v$ on D .

Theorem 7. Let $Lu = q$ in a bounded domain D , where L is parabolic, $c \leq 0$ and $u \in C^0(\bar{D}) \cap C^2(D)$. Then

$$\sup_D |u| \leq \sup_\Sigma |u| + C \sup_D \frac{|q|}{\lambda}, \quad (89)$$

where C is a constant depending only on $\text{diam } D$ and $\beta = \sup |b|/\lambda$.

Proof. (Theorem 7) Let D lie in the slab $0 < x_1 < d$. Without loss of generality, we assume $\lambda_1 \geq \lambda > 0$. Set $L_0 = -\frac{\partial}{\partial t} + a^{ij} \frac{\partial^2}{\partial x_i \partial x_j} + b^i \frac{\partial}{\partial x_i}$. For $\alpha \geq \beta + 1$, we have

$$L_0 e^{\alpha x_1} = (\alpha^2 a^{11} + \alpha b^1) e^{\alpha x_1} \geq \lambda (\alpha^2 - \alpha \beta) e^{\alpha x_1} \geq \lambda \quad (90)$$

Consider the case when $Lu \geq q$. Let

$$v = \sup_\Sigma u^+ + (e^{\alpha d} - e^{\alpha x_1}) \sup_D \frac{|q^-|}{\lambda}, \quad (91)$$

where $u^+ = \max(u, 0)$ and $q^- = \min(q, 0)$. Then, since $Lv = L_0 v + cv \leq -\lambda \sup_\Sigma (|q^-|/\lambda)$ by maximum principle (Corollary 2), we have

$$L(v - u) \leq -\lambda \left(\sup_D \frac{|q^-|}{\lambda} + \frac{q}{\lambda} \right) \leq 0 \text{ in } D, \quad (92)$$

and $v - u \geq 0$ on Σ . Hence, from comparison principle (Corollary 3) we have

$$\sup_D u \leq \sup_D v \leq \sup_\Sigma |u| + C \sup_D \frac{|q|}{\lambda} \quad (93)$$

with $C = e^{\alpha d} - 1$. Consider $Lu \leq q$, we can get similar results with flipped signs. Combine both cases we have for $Lu = q$

$$\sup_D |u| \leq \sup_\Sigma |u| + C \sup_D \frac{|q|}{\lambda}. \quad (94)$$

■

Theorem 8. Suppose that $D \in \mathbb{R}^{d+1}$ is a bounded domain, L is the parabolic operator defined in (84) and $u \in C^0(\bar{D}) \cap C^2(D)$ is a solution to the risk probability PDE. If the PINN F_θ satisfies the following conditions:

- 1) $\sup_{(x,T) \in \Sigma} |F_\theta(x, T) - \tilde{u}(x, T)| < \delta_1$;
- 2) $\sup_{(x,T) \in D} |W_{F_\theta}(x, T)| < \delta_2$;
- 3) $F_\theta \in C^0(\bar{D}) \cap C^2(D)$,

Then the error of F_θ over Ω is bounded by

$$\sup_{(x,T) \in D} |F_\theta(x, T) - u(x, t)| \leq \delta_1 + C \frac{\delta_2}{\lambda} \quad (95)$$

where C is a constant depending on D and L .

Proof. (Theorem 8) Denote $h_1 = L[F_\theta] - q$, and $h_2 = F_\theta - u$. Since F_θ and u both fall in $C^0(\bar{D}) \cap C^2(D)$, from Theorem 7 we have

$$\begin{aligned} \sup_D |h_2(x, t)| &\leq \sup_\Sigma |h_2(x, t)| + C \sup_D \frac{|h_1(x, t)|}{\lambda} \\ &\leq \delta_1 + C \frac{\delta_2}{\lambda} \end{aligned} \quad (96)$$

which gives (95). ■

Lemma 5. Let $D \subset \mathbb{R}^{d+1}$ be a domain. Define the regularity of D as

$$R_D := \inf_{(x,T) \in D, r > 0} \frac{|B(x, T, r) \cap D|}{\min \left\{ |D|, \frac{\pi^{(d+1)/2} r^{d+1}}{\Gamma((d+1)/2 + 1)} \right\}}, \quad (97)$$

where $B(x, T, r) := \{y \in \mathbb{R}^{d+1} \mid \|y - (x, T)\| \leq r\}$ and $|S|$ is the Lebesgue measure of a set S . Suppose that D is bounded and $R_D > 0$. Let $q \in C^0(\bar{D})$ be an l_0 -Lipschitz continuous function on \bar{D} . Then

$$\begin{aligned} \sup_D |q| &\leq \max \left\{ \frac{2 \|q\|_{L_1(\bar{D})}}{R_D |D|}, \right. \\ &\quad \left. 2l_0 \cdot \left(\frac{\|q\|_{L_1(\bar{D})} \cdot \Gamma((d+1)/2 + 1)}{l_0 R_D \cdot \pi^{(d+1)/2}} \right)^{\frac{1}{d+2}} \right\}. \end{aligned} \quad (98)$$

Proof. (Lemma 5) According to the definition of l -Lipschitz continuity, we have

$$l\|(x, T) - (\bar{x}, \bar{T})\|_2 \geq |q(x, T) - q(\bar{x}, \bar{T})|, \quad \forall (x, T), (\bar{x}, \bar{T}) \in \bar{D}, \quad (99)$$

which follows

$$\begin{aligned} \|q\|_{L_1(\bar{D})} &\geq \int_{D^+} |q(x, T)| dx dT \\ &\geq \int_{D^+} |f(\bar{x}, \bar{T})| - l\|(x, T) - (\bar{x}, \bar{T})\| dx dT, \end{aligned} \quad (100)$$

where $D^+ := \{(x, T) \in \bar{D} \mid |q(\bar{x}, \bar{T})| - l\|(x, T) - (\bar{x}, \bar{T})\| \geq 0\}$. Without loss of generality, we assume that $(\bar{x}, \bar{T}) \in \arg \max_{\bar{D}} |q|$ and $q(\bar{x}, \bar{T}) > 0$. Denote that

$$B_1 := B\left(\bar{x}, \bar{T}, \frac{q(\bar{x}, \bar{T})}{2l}\right) \cap D. \quad (101)$$

It obvious that $B_1 \subset D^+$. Note that the Lebesgue measure of a hypersphere in \mathbb{R}^{d+1} with radius r is $\pi^{(d+1)/2} r^{d+1} / \Gamma((d+1)/2 + 1)$. Then (100) becomes

$$\begin{aligned} \|q\|_{L_1(\bar{D})} &\geq \int_{B_1} q(\bar{x}) - l\|(x, T) - (\bar{x}, \bar{T})\| dx dT \\ &\geq |B_1| \cdot \frac{q(\bar{x}, \bar{T})}{2} \\ &\geq \frac{q(\bar{x}, \bar{T})}{2} \cdot R_D \cdot \min \left\{ |D|, \frac{\pi^{(d+1)/2} q(\bar{x}, \bar{T})^{d+1}}{2^{d+1} l^{d+1} \Gamma((d+1)/2 + 1)} \right\} \\ &= \sup_D |q| \cdot \frac{R_D}{2} \cdot \min \left\{ |D|, \frac{\pi^{(d+1)/2} q(\bar{x}, \bar{T})^{d+1}}{2^{d+1} l^{d+1} \Gamma((d+1)/2 + 1)} \right\}, \end{aligned} \quad (102)$$

which leads to (98). ■

Now we are ready to prove Theorem 5.

Proof. (Theorem 5) From condition 1, \mathbf{Y} is uniformly sampled from Σ . From condition 2, \mathbf{X} is uniformly sampled from D . Then we have

$$\mathbb{E}_{\mathbf{Y}} [|F_{\theta}(\mathbf{Y}) - \tilde{u}(\mathbf{Y})|] = \|F_{\theta}(x, T) - \tilde{u}(x, T)\|_{L_1(\Sigma)} / |\Sigma|, \quad (103)$$

$$\mathbb{E}_{\mathbf{X}} [|W_{F_{\theta}}(\mathbf{X})|] = \|W_{F_{\theta}}(x, T)\|_{L_1(D)} / |D|. \quad (104)$$

From condition 1 and 2 we know that

$$\|F_{\theta}(x, T) - \tilde{u}(x, T)\|_{L_1(\Sigma)} < \delta_1 |\Sigma| \quad (105)$$

$$\|W_{F_{\theta}}(x, T)\|_{L_1(D)} < \delta_2 |D| \quad (106)$$

Also from condition 3 we have that $F_{\theta} - \tilde{u}$ and $W_{F_{\theta}}$ are both l -Lipschitz continuous on \bar{D} . From Lemma 5 we know that

$$\begin{aligned} &\sup_{(x, T) \in \Sigma} |F_{\theta}(x, T) - \tilde{u}(x, T)| \\ &\leq \max \left\{ \frac{2\|F_{\theta}(x, T) - \tilde{u}(x, T)\|_{L_1(\Sigma)}}{R_{\Sigma} |\Sigma|}, \right. \\ &\quad \left. 2l \cdot \left(\frac{\|F_{\theta}(x, T) - \tilde{u}(x, T)\|_{L_1(\Sigma)} \cdot \Gamma(d/2 + 1)}{l R_{\Sigma} \cdot \pi^{d/2}} \right)^{\frac{1}{d+1}} \right\} \end{aligned} \quad (107)$$

$$\begin{aligned} &< \max \left\{ \frac{2\delta_1 |\Sigma|}{R_{\Sigma} |\Sigma|}, 2l \cdot \left(\frac{\delta_1 |\Sigma| \cdot \Gamma(d/2 + 1)}{l R_{\Sigma} \cdot \pi^{d/2}} \right)^{\frac{1}{d+1}} \right\}, \\ &\sup_{(x, T) \in D} |W_{F_{\theta}}(x, T)| \\ &\leq \max \left\{ \frac{2\|W_{F_{\theta}}(x, T)\|_{L_1(D)}}{R_D |D|}, \right. \\ &\quad \left. 2l \cdot \left(\frac{\|W_{F_{\theta}}(x, T)\|_{L_1(D)} \cdot \Gamma((d+1)/2 + 1)}{l R_D \cdot \pi^{(d+1)/2}} \right)^{\frac{1}{d+2}} \right\} \\ &< \max \left\{ \frac{2\delta_2 |D|}{R_D |D|}, 2l \cdot \left(\frac{\delta_2 |D| \cdot \Gamma((d+1)/2 + 1)}{l R_D \cdot \pi^{(d+1)/2}} \right)^{\frac{1}{d+2}} \right\}. \end{aligned} \quad (108)$$

Let

$$\begin{aligned}\tilde{\delta}_1 &= \max \left\{ \frac{2\delta_1|\Sigma|}{R_\Sigma|\Sigma|}, 2l \cdot \left(\frac{\delta_1|\Sigma| \cdot \Gamma(d/2+1)}{lR_\Sigma \cdot \pi^{d/2}} \right)^{\frac{1}{d+1}} \right\}, \\ \tilde{\delta}_2 &= \max \left\{ \frac{2\delta_2|D|}{R_D|D|}, 2l \cdot \left(\frac{\delta_2|D| \cdot \Gamma((d+1)/2+1)}{lR_D \cdot \pi^{(d+1)/2}} \right)^{\frac{1}{d+2}} \right\}.\end{aligned}\tag{109}$$

Then from Theorem 8 we know that

$$\sup_{(x,T) \in D} |F_\theta(x,T) - u(x,T)| \leq \tilde{\delta}_1 + C \frac{\tilde{\delta}_2}{\lambda}.\tag{110}$$

Given that $\lambda = \frac{1}{2}\sigma^2$, replace C with $2C$ we get

$$\sup_{(x,T) \in D} |F_\theta(x,T) - u(x,T)| \leq \tilde{\delta}_1 + C \frac{\tilde{\delta}_2}{\sigma^2},\tag{111}$$

which completes the proof. ■

Proof. (Theorem 6)

The proof is based on [56, Theorem 3.6]. We first introduce some definitions. A generic partial differential equation (PDE) has the form

$$\mathcal{L}[u](x) = p(x), \quad \forall x \in D, \quad \mathcal{B}[u](x) = q(x), \quad \forall x \in \Gamma \subseteq \partial D,\tag{112}$$

where $\mathcal{L}[\cdot]$ is a differential operator and $\mathcal{B}[\cdot]$ could be Dirichlet, Neumann, Robin, or periodic boundary conditions. We define the physics-model loss for the PINN training with data m for a neural network instance h as

$$\begin{aligned}\text{Loss}_m^{\text{PINN}}(h; \lambda) &= \frac{\lambda_r}{m_r} \sum_{i=1}^{m_r} \|\mathcal{L}[h](x_r^i) - a(x_r^i)\|^2 + \\ &\quad \frac{\lambda_b}{m_b} \sum_{i=1}^{m_b} \|\mathcal{B}[h](x_b^i) - b(x_b^i)\|^2,\end{aligned}\tag{113}$$

where $\lambda = [\lambda_r, \lambda_b]$ are hyperparameters.

We now restate the assumptions used in [56].

Assumption 3. [56, Assumption 3.1]

Let $D \in \mathbb{R}^{d+1}$ and $\Gamma \in \mathbb{R}^d$ be the state-time space of interest and a subset of its boundary, respectively. Let μ_r and μ_b be probability distributions defined on D and Γ . Let ρ_r be the probability density of μ_r with respect to $(d+1)$ -dimensional Lebesgue measure on D . Let ρ_b be the probability density of μ_b with respect to d -dimensional Hausdorff measure on Γ . We assume the following conditions.

- 1) D is at least of class $C^{0,1}$.
- 2) ρ_r and ρ_b are supported on D and Γ , respectively. Also, $\inf_D \rho_r > 0$ and $\inf_\Gamma \rho_b > 0$.
- 3) For $\epsilon > 0$, there exists partitions of D and Γ , $\{D_j^\epsilon\}_{j=1}^{K_r}$ and $\{\Gamma_j^\epsilon\}_{j=1}^{K_b}$ that depend on ϵ such that for each j , there are cubes $H_\epsilon(\mathbf{z}_{j,r})$ and $H_\epsilon(\mathbf{z}_{j,b})$ of side length ϵ centered at $\mathbf{z}_{j,r} \in D_j^\epsilon$ and $\mathbf{z}_{j,b} \in \Gamma_j^\epsilon$, respectively, satisfying $D_j^\epsilon \subset H_\epsilon(\mathbf{z}_{j,r})$ and $\Gamma_j^\epsilon \subset H_\epsilon(\mathbf{z}_{j,b})$.
- 4) There exists positive constants c_r, c_b such that $\forall \epsilon > 0$, the partitions from the above satisfy $c_r \epsilon^d \leq \mu_r(D_j^\epsilon)$ and $c_b \epsilon^{d-1} \leq \mu_b(\Gamma_j^\epsilon)$ for all j . There exists positive constants C_r, C_b such that $\forall x_r \in D$ and $\forall x_b \in \Gamma$, $\mu_r(B_\epsilon(x_r) \cap D) \leq C_r \epsilon^d$ and $\mu_b(B_\epsilon(x_b) \cap \Gamma) \leq C_b \epsilon^{d-1}$ where $B_\epsilon(x)$ is a closed ball of radius ϵ centered at x . Here C_r, c_r depend only on (D, μ_r) and C_b, c_b depend only on (Γ, μ_b) .
- 5) When $d = 1$, we assume that all boundary points are available. Thus, no random sample is needed on the boundary.

Assumption 4. [56, Assumption 3.2]

Let k be the highest order of the derivative for the PDE of interest. For some $0 < \alpha \leq 1$, let $p \in C^{0,\alpha}(D)$ and $q \in C^{0,\alpha}(\Gamma)$.

- 1) For each training dataset m , let \mathcal{H}_m be a class of neural networks in $C^{k,\alpha}(D) \cap C^{0,\alpha}(\bar{D})$ such that for any $h \in \mathcal{H}_m$, $\mathcal{L}[h] \in C^{0,\alpha}(D)$ and $\mathcal{B}[h] \in C^{0,\alpha}(\Gamma)$.
- 2) For each m , \mathcal{H}_m contains a network u_m^* satisfying $\text{Loss}_m^{\text{PINN}}(u_m^*; \lambda) = 0$.
- 3) And,

$$\sup_m [\mathcal{L}[u_m^*]]_{\alpha;D} < \infty, \quad \sup_m [\mathcal{B}[u_m^*]]_{\alpha;\Gamma} < \infty.$$

We also know that safety-related PDEs are second-order linear parabolic equations. Let U be a bounded domain in \mathbb{R}^d and let $U_T = U \times (0, T]$ for some fixed time $T > 0$. Let (x, t) be a point in \mathbb{R}^{d+1} . For a parabolic PDE, we define

$$\begin{cases} -u_t + L[u] = s, & \text{in } U_T \\ u = \varphi, & \text{in } \partial U \times [0, T] \\ u = v, & \text{in } \bar{U} \times \{t = 0\} \end{cases} \quad (114)$$

where $s : U_T \mapsto \mathbb{R}$, $v : \bar{U} \mapsto \mathbb{R}$, $\varphi : \partial U \times [0, T] \mapsto \mathbb{R}$, and

$$\begin{aligned} L[u] = & \sum_{i,j=1}^d D_i (a^{ij}(x, t) D_j u + b^i(x, t) u) \\ & + \sum_{i=1}^d c^i(x, t) D_i u + d(x, t) u. \end{aligned} \quad (115)$$

Assumption 5. [56, Assumption 3.4]

Let $\lambda(x, t)$ be the minimum eigenvalues of $[a^{ij}(x, t)]$ and $\alpha \in (0, 1)$. Suppose a^{ij}, b^i are differentiable and let $\tilde{b}^i(x, t) = \sum_{j=1}^d D_j a^{ij}(x, t) + b^i(x, t) + c^i(x, t)$ and $\tilde{c}(x, t) = \sum_{i=1}^d D_i b^i(x, t) + d(x, t)$. Let $\Omega = U \times (0, T)$.

- 1) For some constant λ_0 , $\lambda(x, t) \geq \lambda_0 > 0$ for all $(x, t) \in \Omega$.
- 2) $a^{ij}, \tilde{b}^i, \tilde{c}^i$ are Hölder continuous (exponent α) in Ω , and $|a^{ij}|_\alpha, |\tilde{b}^i|_\alpha, |\tilde{c}^i|_\alpha$ are uniformly bounded.
- 3) s is Hölder continuous (exponent α) in U_T and $|d^2 f|_\alpha < \infty$. v and φ are Hölder continuous (exponent α) on $\bar{U} \times \{t = 0\}$, and $\partial U \times [0, T]$, respectively, and $v(x) = \varphi(x, 0)$ on ∂U .
- 4) There exists $\theta > 0$ such that $\theta^2 a^{11}(x, t) + \theta \tilde{b}^1(x, t) \geq 1$ in Ω .
- 5) For $x' \in \partial U$, there exists a closed ball \bar{B} in \mathbb{R}^d such that $\bar{B} \cap \bar{U} = \{x'\}$.
- 6) There are constants $\Lambda, v \geq 0$ such that for all $(x, t) \in \Omega$

$$\begin{aligned} \sum_{i,j} |a^{ij}(x, t)|^2 & \leq \Lambda, \\ \lambda_0^{-2} (\|\mathbf{b}(x, t)\|^2 + \|\mathbf{c}(x, t)\|^2) + \lambda_0^{-1} |d(x, t)| & \leq v^2, \end{aligned} \quad (116)$$

where $\mathbf{b}(x, t) = [b^1(x, t), \dots, b^d(x, t)]^T$ and $\mathbf{c}(x, t) = [c^1(x, t), \dots, c^d(x, t)]^T$.

Now that we have listed all assumptions needed in [56, Theorem 3.6], we are ready to prove Theorem 6.

Note that conditions 1-5 in Assumption 2 match with Assumption 3 ([56, Assumption 3.1]), thus it is satisfied.

Since we assume for any training data set m_r , architecture-wise the physics-informed neural network has enough representation power to characterize the solution of the safety-related PDE u , Assumption 4 ([56, Assumption 3.2]) is satisfied.

For Assumption 5 ([56, Assumption 3.4]), condition 1 is satisfied because we assume the noise magnitude σ has non-zero eigenvalues in Assumption 1, and $a(x, t) = \sigma^\top \sigma$ which indicates all eigenvalues of a are greater than 0, thus λ_0 can be found and this condition is satisfied. For condition 2, we have f, g and σ in the system dynamics are bounded and continuous from Assumption 1, and we know $a = \sigma^\top \sigma$, $b \equiv 0$, $c = f + g u_{\text{nominal}}$ and $d \equiv 0$. Thus, $a^{ij}, \tilde{b}^i, \tilde{c}^i$ are Hölder continuous (exponent α) in Ω , and $|a^{ij}|_\alpha, |\tilde{b}^i|_\alpha, |\tilde{c}^i|_\alpha$ are uniformly bounded, indicating the condition is satisfied. For condition 3, we know that $s \equiv 0$ and $\varphi \equiv 0$ or $\varphi \equiv 1$, and $v \equiv 0$ or $v \equiv 1$ depending on the specific choice of the safety-related probability, thus they are Hölder continuous and we know that condition 3 is satisfied. For condition 4, since we have $a^{11} > 0$ in Assumption 1 and we know $b \equiv 0$, we can always find $\theta > 0$ so that the condition is satisfied. For condition 5, it is assumed in the regularity condition in Assumption 2 thus is satisfied. For condition 6, we have f, g, σ bounded in Assumption 1 and we know that $a = \sigma^\top \sigma$, $b \equiv 0$, $c = f + g u_{\text{nominal}}$ and $d \equiv 0$. Thus, we can find constants $\Lambda, v \geq 0$ to bound $\sum_{i,j} |a^{ij}(x, t)|^2$ and $\lambda_0^{-2} (\|\mathbf{b}(x, t)\|^2 + \|\mathbf{c}(x, t)\|^2) + \lambda_0^{-1} |d(x, t)|$ for all $(x, t) \in \Omega$, indicating this condition is satisfied.

Till here, we have shown that all assumptions needed in [56, Theorem 3.6] are satisfied. As the number of training data $m_r \rightarrow \infty$, the loss function (23) is equivalent to the Hölder regularized empirical loss [56, Equation (3.3)]. Thus, all conditions in [56, Theorem 3.6] hold and we have

$$\lim_{m_r \rightarrow \infty} F_{m_r} = u.$$

■

In the following sections, we provide details for the experiments presented in the paper and some additional experiments.

D. Generalization to unseen regions

In the generalization task in section VII-A, we use a down-sampled sub-region of the system to train the proposed PIPE framework, and test the prediction results on the full state-time space. We showed that PIPE is able to give accurate inference on the entire state space, while standard fitting strategies cannot make accurate predictions. In the paper, we only show the fitting results of thin plate spline interpolation. Here, we show the results of all fitting strategies we tested for this generalization tasks. The fitting strategies are

- 1) Polynomial fitting of 5 degrees for both state x and time T axes. The fitting sum of squares error (SSE) on the training data is 0.1803.
- 2) Lowess: locally weighted scatterplot smoothing [63]. The training SSE is 0.0205.
- 3) Cubic spline interpolation. The training SSE is 0.
- 4) Biharmonic spline interpolation. The training SSE is 2.52×10^{-27} .
- 5) TPS: thin plate spline interpolation. The training SSE is 1.64×10^{-26} .

All fittings are conducted via the MATLAB Curve Fitting Toolbox. Fig. 7 visualizes the fitting results on the full state space. Polynomial fitting performs undesirably because the polynomial functions cannot capture the risk probability geometry well. Lowess fitting also fails at inference since it does not have any model information of the data. Given the risk probability data, cubic spline cannot extrapolate outside the training region, and we use 0 value to fill in the unseen region where it yields NAN for prediction. Biharmonic and TPS give similar results as they are both spline interpolation methods. None of these fitting methods can accurately predict the risk probability in unseen regions, because they purely rely on training data and do not incorporate any model information of the risk probability for prediction.

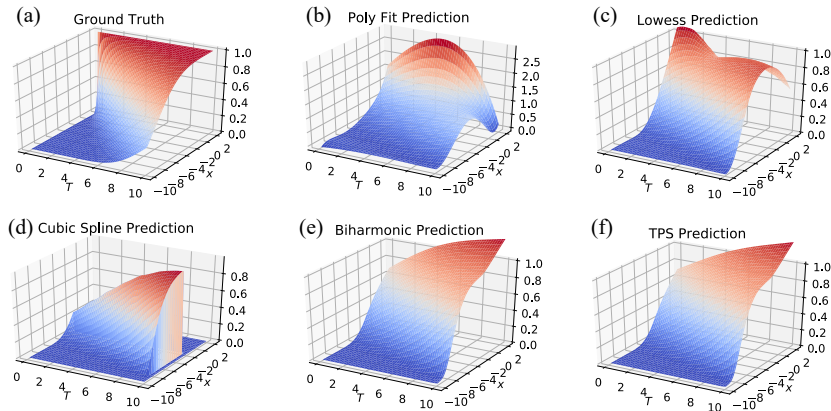


Fig. 7: Results of different fitting strategies on the risk probability generalization task.

We also compare the prediction results for different network architectures in the proposed PIPE framework, to examine the effect of network architectures on the risk probability prediction performance. The network settings we consider are different hidden layer numbers (1-4) and different numbers of neurons in one hidden layer (16, 32, 64). We use 3 hidden layers, 32 neurons per layer as baseline (the one used in the paper). Table I and Table II report the averaged absolute error of the predictions for different layer numbers and neuron numbers per layer, respectively. We trained the neural networks 10 times with random initialization to report the standard deviation. We can see that as the number of layers increases, the prediction error of the risk probability drops, but in a relatively graceful manner. The prediction error for a single layer PIPE is already very small, which indicates that the proposed PIPE framework is very efficient in terms of computation and storage. The prediction accuracy tends to saturate when the hidden layer number reaches 3, as there is no obvious improvement when we increase the layer number from 3 to 4. This means for the specific task we consider, a 3-layer neural net has enough representation. Under the same layer number, as the neuron number per layer increases, the risk probability prediction error decreases. This indicates that with larger number of neuron in each layer (*i.e.*, wider neural networks), the neural network can better capture the mapping between state-time pair and the risk probability. However, the training time increases significantly for PIPEs with more neurons per layer (152s for 16 neurons and 971s for 64 neurons), and the gain in prediction accuracy becomes marginal compared to the amount of additional computation involved. We suggest to use a moderate number of neurons per layer to achieve desirable trade-offs between computation and accuracy.

# Hidden Layer	1	2	3	4
Prediction Error ($\times 10^{-3}$)	4.773 ± 0.564	2.717 ± 0.241	2.819 ± 0.619	2.778 ± 0.523

TABLE I: Risk probability prediction error of PIPE for different numbers of hidden layers.

# Neurons	16	32	64
Prediction Error ($\times 10^{-3}$)	2.743 ± 0.313	2.931 ± 0.865	2.599 ± 0.351

TABLE II: Risk probability prediction error of PIPE for different neuron numbers per layer.

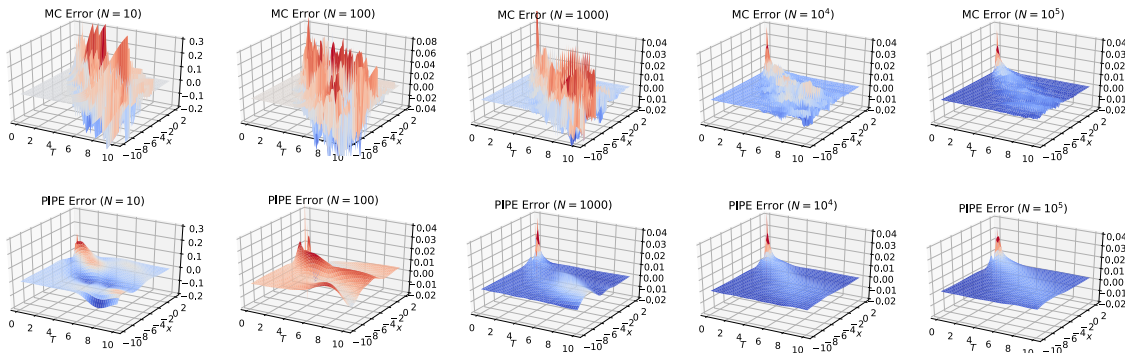


Fig. 8: Prediction errors for Monte Carlo (left) and PIPE (right) with different sample numbers.

E. Efficient estimation of risk probability

In the efficient estimation task in section VII-B, we showed that PIPE will give better sample efficiency in risk probability prediction, in the sense that it achieves the same prediction accuracy with less sample numbers. Here, we visualize the prediction errors of Monte Carlo (MC) and the proposed PIPE framework to better show the results. Fig. 8 shows the prediction error comparison plots for MC and PIPE with different sample numbers N . As the sample number increases, the errors for both MC and PIPE decrease because of better resolution of the data. PIPE gives more accurate predictions than MC across all sample numbers, since it combines data and physical model of the system together. From Fig. 8 we can see that, PIPE indeed provides smoother and more accurate estimation of the risk probability. The visualization results further validate the efficacy of the proposed PIPE framework.

# Hidden Layer	1	2	3	4
Prediction Error ($\times 10^{-4}$)	14.594 ± 2.109	7.302 ± 0.819	6.890 ± 0.613	6.625 ± 0.574

TABLE III: Risk probability gradient prediction error of PIPE for different numbers of hidden layers.

F. Adaptation on changing system parameters

For the adaptation task described in section VII-C, we trained PIPE with system data of parameters $\lambda_{\text{train}} = [0.1, 0.5, 0.8, 1]$ and tested over a range of unseen parameters over the interval $\lambda = [0, 2]$. Here, we show additional results on parameters $\lambda_{\text{test}} = [0.3, 0.7, 1.2, 2]$ to further illustrate the adaptation ability of PIPE. Fig. 9 shows the results. It can be seen that PIPE is able to predict the risk probability accurately on both system parameters with very low error over the entire state-time space. This result indicates that PIPE has solid adaptation ability on uncertain parameters, and can be used for stochastic safe control with adaptation requirements.

G. Estimating the gradient of risk probability

For the gradient estimation task in section VII-D, we presented that PIPE is able to predict the risk probability gradients accurately by taking finite difference on the predicted risk probabilities. This result shows that PIPE can be used for first- and higher-order methods for safe control, by providing accurate gradient estimations in a real-time fashion. Similar to the generalization task, here we report the gradient prediction errors with different network architectures in PIPE, to examine the effect of network architectures on the gradient estimation performance. Table III and Table IV show the averaged absolute error of gradient predictions for different layer numbers and neuron numbers per layer. We trained the neural networks for 10 times with random initialization to report the standard deviation. We can see that as the number of hidden layer increases, the gradient prediction error keeps dropping, and tends to saturate after 3 layers. With the increasing neuron numbers per layer, the gradient prediction error decreases in a graceful manner. Similar to the generalization task, larger networks with more hidden

# Neurons	16	32	64
Prediction Error ($\times 10^{-4}$)	7.049 ± 0.767	6.890 ± 0.613	6.458 ± 0.794

TABLE IV: Risk probability gradient prediction error of PIPE for different neuron numbers per layer.

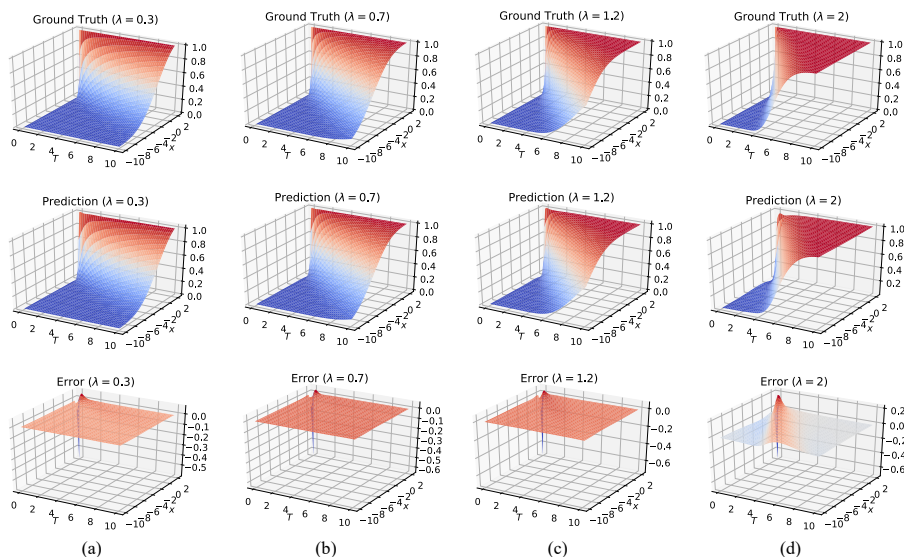


Fig. 9: Risk probability prediction results on systems with unseen parameters $\lambda_{\text{test}} = [0.3, 0.7, 1.2, 2]$.

layers and more neurons per layer can give more accurate estimation of the gradient, but the computation time scales poorly compared to the accuracy gain. Based on these results, we suggest to use moderate numbers of layers and neurons per layer to acquire desirable gradient prediction with less computation time.

In this section, we provide additional experiment results on risk estimation of the inverted pendulum on a cart system, as well as safe control with risk estimation through the proposed PIPE framework.

H. Risk estimation of inverted pendulum on a cart system

We consider the inverted pendulum on a cart system, with dynamics given by

$$\frac{d\mathbf{x}}{dt} = f(\mathbf{x}) + g(\mathbf{x})u + \sigma \tilde{I} dW_t, \quad (117)$$

where $\mathbf{x} = [x, \dot{x}, \theta, \dot{\theta}]^\top$ is the state of the system and $u \in \mathbb{R}$ is the control, with x and \dot{x} being the position and velocity of the cart, and θ and $\dot{\theta}$ being the angle and angular velocity of the pendulum. We use \mathbf{x} to denote the state of the system to distinguish from cart's position x . Then, we have

$$f(\mathbf{x}) = \begin{bmatrix} 1 & 0 & 0 & 0 \\ 0 & m + M & 0 & ml \cos \theta \\ 0 & 0 & 1 & 0 \\ 0 & ml \cos \theta & 0 & ml^2 \end{bmatrix}^{-1} \begin{bmatrix} \dot{x} \\ ml\dot{\theta}^2 \sin \theta - b_x \dot{x} \\ \dot{\theta} \\ mgl \sin \theta - b_\theta \dot{\theta} \end{bmatrix}, \quad (118)$$

$$g(\mathbf{x}) = \begin{bmatrix} 1 & 0 & 0 & 0 \\ 0 & m + M & 0 & ml \cos \theta \\ 0 & 0 & 1 & 0 \\ 0 & ml \cos \theta & 0 & ml^2 \end{bmatrix}^{-1} \begin{bmatrix} 0 \\ 1 \\ 0 \\ 0 \end{bmatrix}, \quad (119)$$

where m and M are the mass of the pendulum and the cart, g is the acceleration of gravity, l is the length of the pendulum, and b_x and b_θ are constants. The last term in (117) is the additive noise, where W_t is 4-dimensional Wiener process with $W_0 = \mathbf{0}$, σ is the magnitude of the noise, and

$$\tilde{I} = \begin{bmatrix} 0 & 0 & 0 & 0 \\ 0 & 1 & 0 & 0 \\ 0 & 0 & 0 & 0 \\ 0 & 0 & 0 & 1 \end{bmatrix}. \quad (120)$$

Fig. 10 visualizes the system.

The safe set is defined in (3) with barrier function $\phi(\mathbf{x}) = 1 - (\frac{\mathbf{x}_3}{\pi/3})^2 = 1 - (\frac{\theta}{\pi/3})^2$. Essentially the system is safe when the angle of the pendulum is within $[-\pi/3, \pi/3]$. We consider spatial-temporal space $\Omega \times \tau = [[-10, 10] \times [-\pi/3, \pi/3] \times [-\pi, \pi] \times [0, 1]$. We collect training and testing data on $\Omega \times \tau$ with grid size $N_{\Omega\text{-train}} = 13$ and $N_{\tau\text{-train}} = 10$ for training and $N_{\Omega\text{-test}} = 25$ and $N_{\tau\text{-test}} = 10$ for testing. The nominal controller we choose is a proportional controller $N(\mathbf{x}) = -K\mathbf{x}$ with $K =$

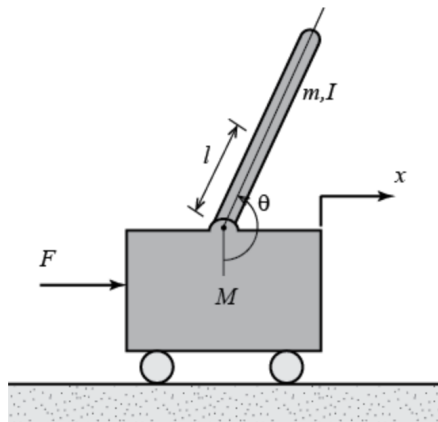


Fig. 10: Inverted pendulum on a cart.

Parameters	Values
M	1
m	0.1
g	9.8
l	0.5
b_x	0.05
b_θ	0.1

TABLE V: Parameters used in the inverted pendulum simulation.

$[0, -0.9148, -22.1636, -14.3992]^\top$. The sample number for MC simulation is set to be $N = 1000$ for both training and testing. Table V lists the parameters used in the simulation.

We train PIPE with the same configuration listed in section VII. According to Theorem 1, the PDE that characterizes the safety probability of the pendulum system is

$$\frac{\partial F}{\partial T}(\mathbf{x}, T) = (f(\mathbf{x}) - g(\mathbf{x})K\mathbf{x}) \frac{\partial F}{\partial \mathbf{x}}(\mathbf{x}, T) + \frac{1}{2}\sigma^2 \tilde{I} \text{tr} \left(\frac{\partial^2 F}{\partial \mathbf{x}^2}(\mathbf{x}, T) \right), \quad (121)$$

which is a high dimensional and highly nonlinear PDE that cannot be solved effectively using standard solvers. Here we can see the advantage of combining data with model and using a learning-based framework to estimate the safety probability. Fig. 11, Fig. 12 and Fig. 13 show the results of the PIPE predictions. We see that despite the rather high dimension and nonlinear dynamics of the pendulum system, PIPE is able to predict the safety probability of the system with high accuracy. Besides, since PIPE takes the model knowledge into training loss, the resulting safety probability prediction is smoother thus more reliable than pure MC estimations.

I. Safe control with PIPE

We consider the control affine system (1) with $f(x) \equiv Ax = 2x$, $g(x) \equiv 1$, $\sigma(x) \equiv 2$. The safe set is defined as in (3) and the barrier function is chosen to be $\phi(x) := x - 1$. The safety specification is given as the forward invariance condition. The nominal controller is a proportional controller $N(x) = -Kx$ with $K = 2.5$. The closed-loop system with this controller has

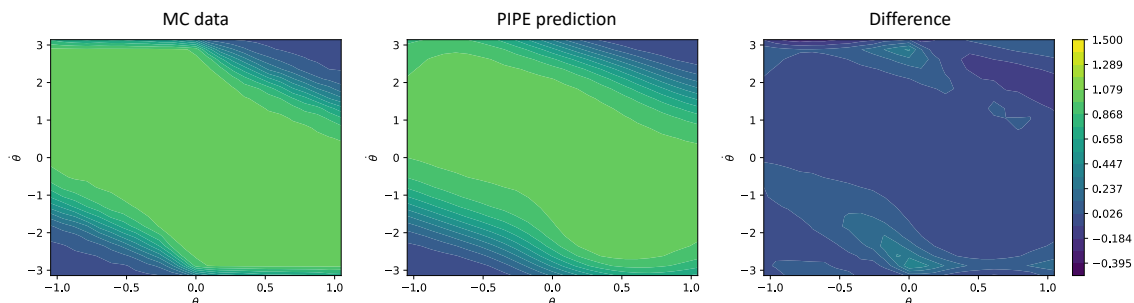


Fig. 11: Safety probability from MC simulation and PIPE prediction, and their difference. Results on outlook time horizon $T = 0.6$, initial velocity $v = 0$. The x-axis shows the initial angle, and y-axis shows the initial angular velocity.

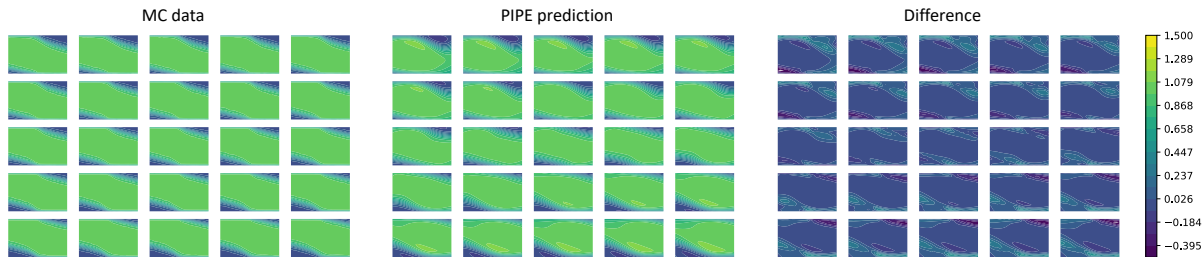


Fig. 12: Safety probability from MC simulation and PIPE prediction, and their difference. Results on outlook time horizon $T = 0.3$. The 5x5 plots show results on 25 different initial velocities uniformly sampled in $[-10, 10]$. The x-axis and y-axis (omitted) are the initial angle and the initial angular velocity as in Fig. 11. One can see that the safety probability shift as the velocity changes, and the safety probability is symmetric with regard to the origin $v = 0$ due to the symmetry of the dynamics.

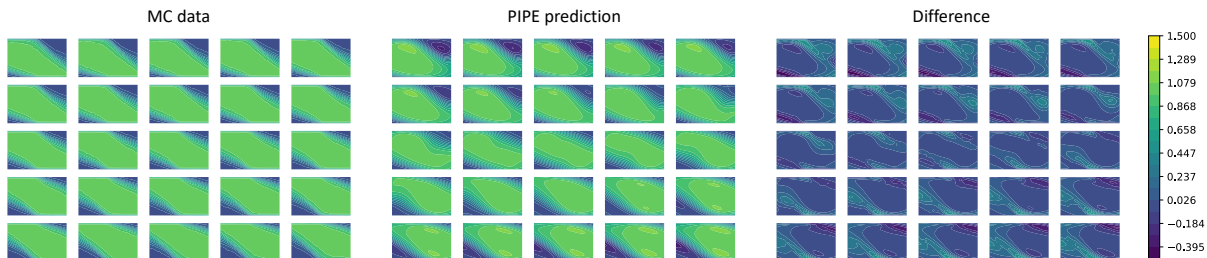


Fig. 13: Safety probability from MC simulation and PIPE prediction, and their difference. Results on outlook time horizon $T = 1$. The 5x5 plots show results on 25 different initial velocities uniformly sampled in $[-10, 10]$.

an equilibrium at $x = 0$ and tends to move into the unsafe set in the state space. We run simulations with $dt = 0.1$ for all controllers. The initial state is set to be $x_0 = 3$. For this system, the safety probability satisfies the following PDE

$$\frac{\partial F}{\partial T}(x, T) = -0.5x \frac{\partial F}{\partial x}(x, T) + 2 \text{tr} \left(\frac{\partial^2 F}{\partial x^2}(x, T) \right), \quad (122)$$

with initial and boundary conditions

$$\begin{aligned} F(x, t) &= 0, \quad x \leq 1, \\ F(x, 0) &= \mathbb{1}(x \geq 1). \end{aligned} \quad (123)$$

We first estimate the safety probability $F(x, T)$ of the system via PIPE. The training data $\bar{F}(x, T)$ is acquired by running MC on the system dynamics for given initial state x_0 and nominal control N . Specifically,

$$\bar{F}(x, T) = \mathbb{P}(\forall t \in [0, T], x_t \in \mathcal{C} \mid x_0 = x) = \frac{N_{\text{safe}}}{N}, \quad (124)$$

with $N = 100$ being the number of sample trajectories. The training data is sampled on the state-time region $\Omega \times \tau = [1, 10] \times [0, 10]$ with grid size $dx = 0.5$ and $dt = 0.5$. We train PIPE with the same configuration as listed in section VII. We test the estimated safety probability and its gradient on the full state space $\Omega \times \tau$ with $dx = 0.1$ and $dt = 0.1$. Fig. 14 shows the results. It can be seen that the PIPE estimate is very close to the Monte Carlo samples, which validates the efficacy of the framework. Furthermore, the PIPE estimation has smoother gradients, due to the fact that it leverages model information along with the data.

We then show the results of using such estimated safety probability for control. Fig. 15 shows the results. For the baseline stochastic safe controllers for comparison, refer to [41] for details. We see that the PIPE framework can be applied to long-term safe control methods discussed in [41]. Together with the PIPE estimation, long-term safety can be ensured in stochastic control systems.

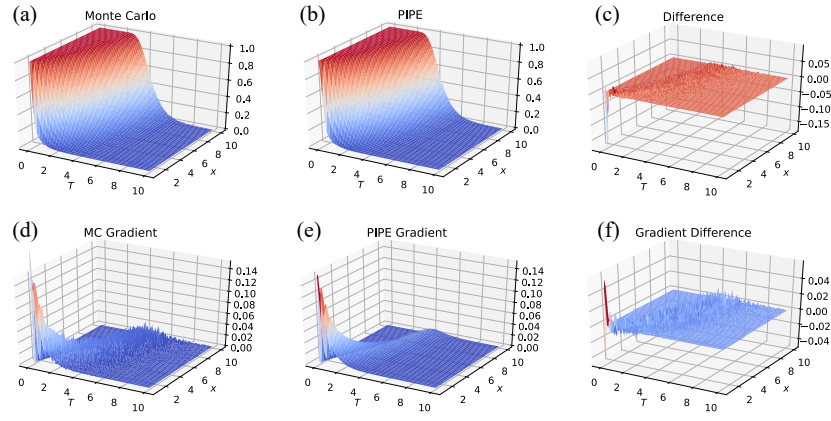


Fig. 14: Safety probability and its gradient of Monte Carlo samples and PIPE estimation.

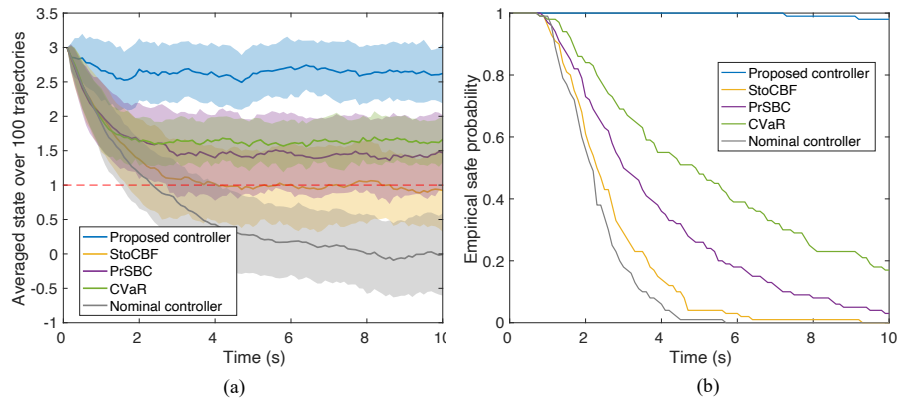


Fig. 15: Safe control with probability estimation from PIPE compared with other baselines.